PHENOMENA THAT DETERMINE KNOCK ONSET IN SPARK-IGNITED ENGINES

by

Bridget M. Revier

B.S., Chemical Engineering
B.S., Chemistry
Rose-Hulman Institute of Technology, 2004

Submitted to the Department of Mechanical Engineering
in Partial Fulfillment of the Requirements for the Degree of

Master of Science in Mechanical Engineering

at the

Massachusetts Institute of Technology

June 2006

Signature of the Author.....
Department of Mechanical Engineering
May 17, 2006

Certified by.....
John B. Heywood
Sun Jae Professor of Mechanical Engineering
Thesis Advisor

Accepted by.....
Lallit Anand
Professor, Department of Mechanical Engineering
Chairman, Department of Graduate Committee

(page intentionally left blank)

PHENOMENA THAT DETERMINE KNOCK ONSET IN SPARK-IGNITED ENGINES

by

Bridget M. Revier

Submitted to the Department of Mechanical Engineering
on May 17, 2006 in Partial Fulfillment of the
Requirements for the Degree of Master of Science in
Mechanical Engineering

ABSTRACT

Experiments were carried out to collect in-cylinder pressure data and microphone signals from a single-cylinder test engine using spark timings before, at, and after knock onset for four different octane-rated toluene reference fuels. This data was then processed and analyzed in various ways to gain insight into the autoignition phenomena that lead to knock. This was done to develop a more fundamentally based prediction methodology that incorporates both a physical and chemical description of knock. The collected data was also used to develop a method of data processing that would detect knock in real time without the need to have an operator listening to the engine.

Bandpass filters and smoothing techniques were used to process the data. The processed data was then used to determine knock intensities for each cycle for both the cylinder pressure data and microphone signal. Also, the rate of build-up before reaching peak amplitude in a bandpass filtered pressure trace was found. A trend was found showing that cycles with knock intensities greater than 1 bar with rapid build-up (5-10 oscillations) before reaching the peak are the type the cycles whose autoignition events lead to engine knock. The cylinder pressure knock intensities and microphone knock intensities were plotted and then fit with a linear trendline. The R^2 value for these linear trendlines will transition from considerably lower values to values greater than 0.85 at the spark timing of knock onset.

It is believed that the higher cylinder pressure knock intensities, in conjunction with the faster build-up of 5-10 oscillations before reaching peak, helps to explain the knock phenomena. It supports conclusions from previous works that the end gas contains one or more hot spots that autoignite in sequence causing pressure gradients that can trigger rapid pressure oscillations. These pressure oscillations can cause block and head vibrations that lead to audible noise outside the engine

Thesis Advisor: John B. Heywood
Title: Sun Jae Professor of Mechanical Engineering

(page intentionally left blank)

I would like to thank my friends, family, and coworkers
for the great deal of support they have provided me
throughout this endeavor.

(page intentionally left blank)

TABLE OF CONTENTS

LIST OF TABLES

(page intentionally left blank)

LIST OF FIGURES

CHAPTER 1: INTRODUCTION

1.1 KNOCK FUNDAMENTALS

Knock is a highly researched area because it is not adequately understood. Many also believe knock to be a significant barrier to greatly improving the performance of spark-ignited gasoline engines through turbocharging. Turbocharging forces more air into the cylinder. This increase in air density causes a turbocharged engine to produce higher brake mean effective pressures (BMEP) without greatly increasing the engine friction. This means that an engine can be downsized while still meeting the same torque requirements and increasing its part load efficiency. This path of turbocharging and downsizing is similar to what has previously been done with diesel engines. The challenge in turbocharging gasoline engines is the increased knock severity. Engine knock is an unacceptable combustion phenomenon for the following two reasons: the sound is unpleasant and undesirable to the passengers in a vehicle, and at a high enough intensity, knock can lead to engine damage.

1.1.1 Knock Definition

Engine knock is a knocking or pinging sound that can be heard outside an operating engine. It is caused by the rapid autoignition of a portion of the in-cylinder charge that generates a local pressure pulse creating pressure oscillations. These oscillation then propagate across the cylinder in a manner which creates noise outside the engine.[1] This autoignition is usually initiated from one or more hot-spots in the end gas, the unburned mixture ahead of the flame front. Not all autoignition events will lead to knock.

Many methods for the detection of knock onset have been explored. A brief list includes the use of processed cylinder pressures, accelerometers to detect engine vibrations, optical detectors, spark plug ionization probes, heat transfer data, as well as microphones and the ear alone. For this work, knock onset is defined as the instant at which a knocking or pinging sound can be heard through a set of headphones attached to a microphone in the test cell. This microphone/headphone setup will be explained in more detail in Section 2.2.8.

1.1.2 Factors that Affect Engine Knock

The thermodynamic state of the end gas in the cylinder is greatly affected by cylinder pressure. An increase in end gas pressure increases end gas temperature which in turn increases reaction rates. Factors that affect cylinder pressure are inlet pressure, air-fuel ratio, spark timing, compression ratio, engine speed, charge preparation, and combustion chamber geometry. Factors that affect end gas temperature and composition are mixture composition and initial temperature. Following is a brief description of each of these factors:

- Inlet pressure: A higher inlet pressure forces a larger amount of air-fuel mixture into the cylinder which increases cylinder pressure and increases engine torque output.
- Air-fuel ratio: Variations in the amount of excess air or excess fuel in the cylinder changes the combustion rates and the energy release which in turn affects cylinder pressure and end gas temperatures.
- Spark timing: Earlier spark timing causes earlier combustion which results in higher cylinder pressures because combustion takes place in a smaller volume. Knock is more likely with an earlier spark timing because the maximum end gas temperature is increased.
- Compression ratio: A higher compression ratio leaves a smaller volume available for combustion which increases cylinder pressure and end gas temperatures.
- Engine speed: A slower engine speed means that each cycle lasts longer resulting in an end gas at a higher pressure and temperature for a longer period of time making an autoignition event more likely to occur.
- Charge preparation: The amount of turbulence, swirl, and tumble affects the homogeneity of the mixture as well as the end gas location in the cylinder.
- Combustion chamber geometry: The general shape of the combustion chamber, as well as spark plug location, affects the flame front area and the distance the flame front must travel. A small flame front or large distance slows combustion increasing the likelihood of an autoignition event.
- Mixture composition: The mixture composition, including air-fuel ratio and residual fraction, affects the ratio of specific heats (γ) as per Equation (1.1).

$$T = T_{init}\left(\frac{P}{P_{init}}\right)^{\left(\frac{\gamma-1}{\gamma}\right)} \tag{1.1}$$

A higher γ, which is caused by a higher air-fuel ratio or a lower residual fraction, leads to higher compression temperatures. The type of fuel and fuel additives can also have an effect.

- Initial temperature: A higher initial temperature leads to a higher compression temperature as shown in Equation (1.1). Initial temperature can be affected by the temperature of the inlet air, heat transfer, and the residual gas fraction and temperature.

1.2 PREVIOUS WORK

While extensive work has been done in the field of engine knock research, this section reviews some of the research that is most relevant to the specific objectives outlined in the next section. Varying definitions and descriptions of knock are also included.

1.2.1 Brief Overview of Knock Detection Methods

Lee, et al. [2] affirmed that cylinder pressure data gives the most accurate information regarding knock; however, they also confirmed that there is a great deal of disagreement on how cylinder pressure data should be processed and used. One method of data processing proposed by this team was to use three narrow bandpass filters for the first, second, and third harmonic knock frequencies. It was mentioned that the results attained, especially that of knock intensity, vary with engine operating conditions, sensor location, and the fuel used. Some of their other suggestions included: using a piece of tubing that is funnel shaped at the ends as a wave guide to pick up the pressure signals with a microphone and also combining audible detection by the ear alone with observation of the vibration signal.

Various measures were used by Kaneyasu, et al. [3] to determine knock onset. These methods included the use of a piezoelectric accelerometer to detect engine vibrations. A cylinder pressure sensor was used in conjunction with the engine vibration data. The

cylinder pressure data was bandpass filtered at the most representative resonant frequency and integrated. Knock intensity was determined by monitoring the signal to noise ratio of the spectra.

Chiriac, Radu, and Apostolescu [4] also used a signal to noise ratio approach for finding the crank angle of knock onset but acknowledged in the paper that there were problems with the use of this method. Instead, they used a plot of knock intensity versus spark timing in order to determine the knock threshold.

1.2.2 Variation in Levels of Pressure Waves

It is not necessary for each individual cycle in an engine to be rapidly autoigniting in order to consider the engine as a whole to be knocking. In fact, it may be possible to achieve full engine knock, under certain circumstances such as when using fuels that have lower octane numbers, with as few as 6% of the cycles rapidly autoigniting.

It is stated in a paper by Grandin, et al. [5] that only autoignition events that cause a fast energy release that produce pressure gradients triggering pressure oscillations at natural frequencies will lead to the noise that generates engine knock.

Bradley and Morley [6] concluded from their studies that the spatial gradient of temperature around the hot spots in the cylinder is important. More specifically, it is the ratio of the temperature gradient in the hot spot to the critical temperature gradient that is important. The critical temperature gradient is defined at the instant when the autoignition front travels at the acoustic speed into the unburned mixture. When this ratio is within a certain range, the major heat release is in the form of an acoustic wave, and this wave may or may not reinforce the chemical wave. The act of these waves reinforcing or canceling each other may differentiate between a knocking and non-knocking individual cycle.

Konig and Sheppard [7] stated a similar proposal in an earlier paper. They state that autoignition occurring late in a cycle does not lead to rapid pressure oscillations but rather acts more like an extension of the main flame. They define autoignition as a

chemical reaction which accelerates to spontaneous, light-emitting ignition and knock as abnormal oscillations in the cylinder pressure during combustion. They also characterized knock by carbon formation and high velocity post-knock gas motions.

1.2.3 Proposed Mechanisms for the Increase in Pressure Oscillation Amplitude

Pan and Sheppard [8] maintain that rather than a single hot spot causing engine knock, multiple hot spots are required. They found that pressure emanating from the first hot spot will modify the temperature gradient around adjacent hot spots. This can lead to the displacement of a second hot spot at a lower temperature by the expansion of the first hot spot. The second hot spot may initially react more slowly than the first but can exhibit a more violent reaction of the developing detonation type which leads to engine knock.

Konig and Sheppard [7] also referenced in their paper a video clip titled *Autoignition and Knock in a SI Engine*. Several figures in this section highlight some of the critical frames in this video clip. These figures feature a natural light film of a moderately knocking cycle. Figure 1. 1 shows the cylinder before autoignition occurs. All that can be seen in this frame is a relatively smooth flame front. Autoignition has begun in Figure 1. 2, and there is an appearance of several hot spots in front of the original flame front from Figure 1. 1. Figure 1. 3 shows the expansion of the end gas throughout the cylinder, and the hot spots still show as lighter areas in the frame. Finally, at the end of the cycle in Figure 1. 4, the lighter areas have spread even further and are less distinct.

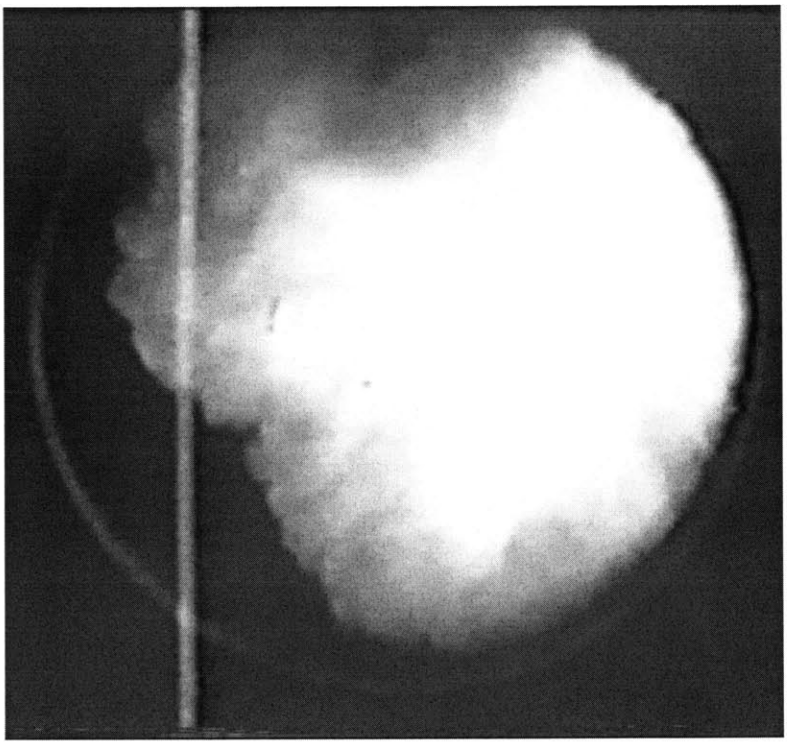

Figure 1. 1: Pre-Autoignition Frame of Moderately Knocking Cycle on Natural Light Film [7]

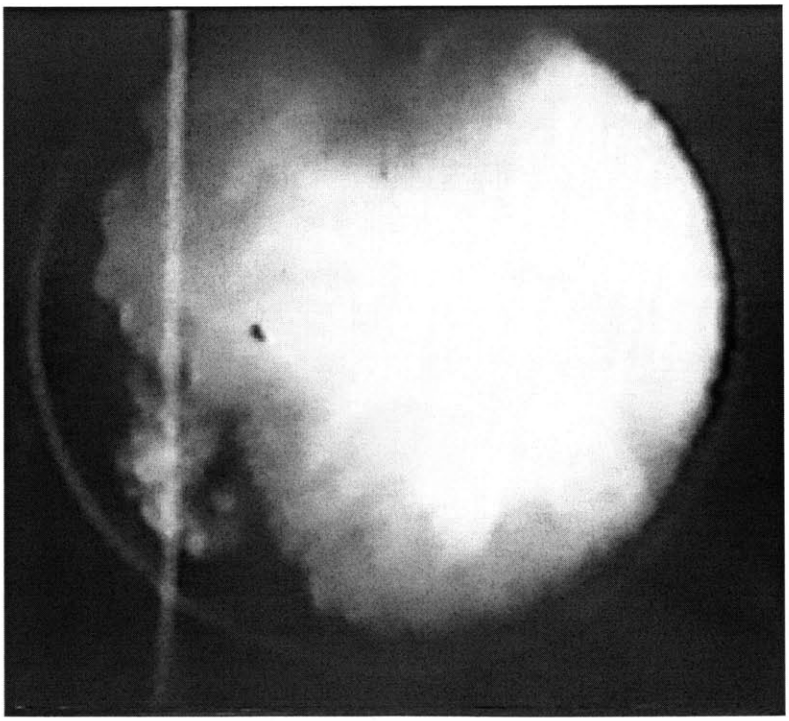

Figure 1. 2: Autoignition Frame of Moderately Knocking Cycle on Natural Light Film [7]

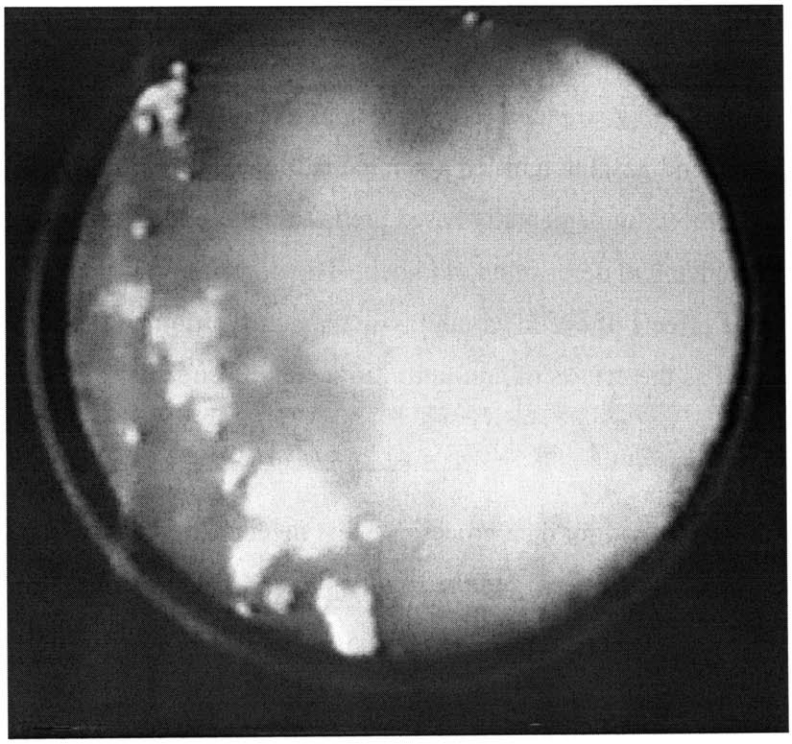

Figure 1. 3: End Gas Expansion Frame of Moderately Knocking Cycle on Natural Light Film [7]

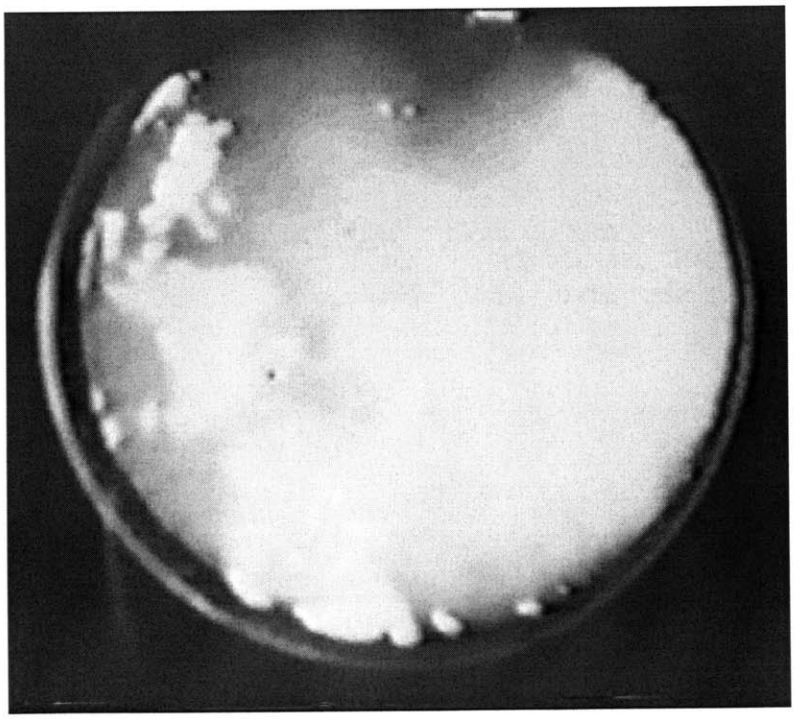

Figure 1. 4: End of Cycle Frame of Moderately Knocking Cycle on Natural Light Film [7]

1.3 RESEARCH OBJECTIVES

The goal of this research was to improve the ability to describe what occurs at the practical knock onset limit. This overall goal included the development of a more complete description that links the end gas autoignition phenomena to the engine knock process and the development of a more fundamentally based prediction methodology that incorporates both a physical and chemical description of knock. The description was to incorporate information about the effects of cyclic variability in the autoignition and pressure wave phenomena as well as the effects of non-uniformities in the end gas temperature and composition.

A secondary goal was to develop a method for data processing that detects knock in real time without the need to have an operator listening to the engine. A knock detection method based on data analysis is more objective and less expensive than an operator.

CHAPTER 2: EXPERIMENTAL METHOD

2.1 TEST CELL SETUP

The test cell consists of a single-cylinder test engine, a variable frequency dynamometer, and various pieces of control and test equipment.

2.1.1 Engine Specifications

The engine used for the experiments contained within this thesis was a single-cylinder test engine. It has a Ricardo MK III base with a Volvo B5254 pent-roof, 4-valve, central spark plug cylinder head. The engine specifications can be found in Table 2. 1.

Table 2. 1: Engine Specifications

Bore	83 mm
Stroke	90 mm
Connecting Rod Length	158 mm
Displacement Volume	487 cm^2
Clearance Volume	55 cm^2
Compression Ratio	9.8:1
Intake Valve Opening	0° BTC
Intake Valve Closing	60° ABC
Exhaust Valve Opening	48° BBC
Exhaust Valve Closing	12° ATC

2.1.2 Dynamometer Specifications

This engine was connected via a drive shaft to an Eaton Dynamatic AF-6360 50hp dynamometer, which was controlled by an Eaton Dynamatic Adjustable Frequency Drive. This motor and drive combination was able to both motor the engine as well as absorb power when the engine was fired. The system was able to automatically adjust the torque output to maintain a constant speed.

2.1.3 Air and Fuel Systems

Air was brought into the intake system through a filter located high in the test cell. It then passed through a laminar flow element with a pressure sensor attached that allows for the calculation of air mass flow rate. After the laminar flow element, the air passed through a damping tank to reduce any pulsations and was then throttled on the way to the engine. The test cell contained the option of switching to a boosted air supply, but this option was not used in any of the testing mentioned here. Figure 2. 1 shows a schematic of the air intake system.

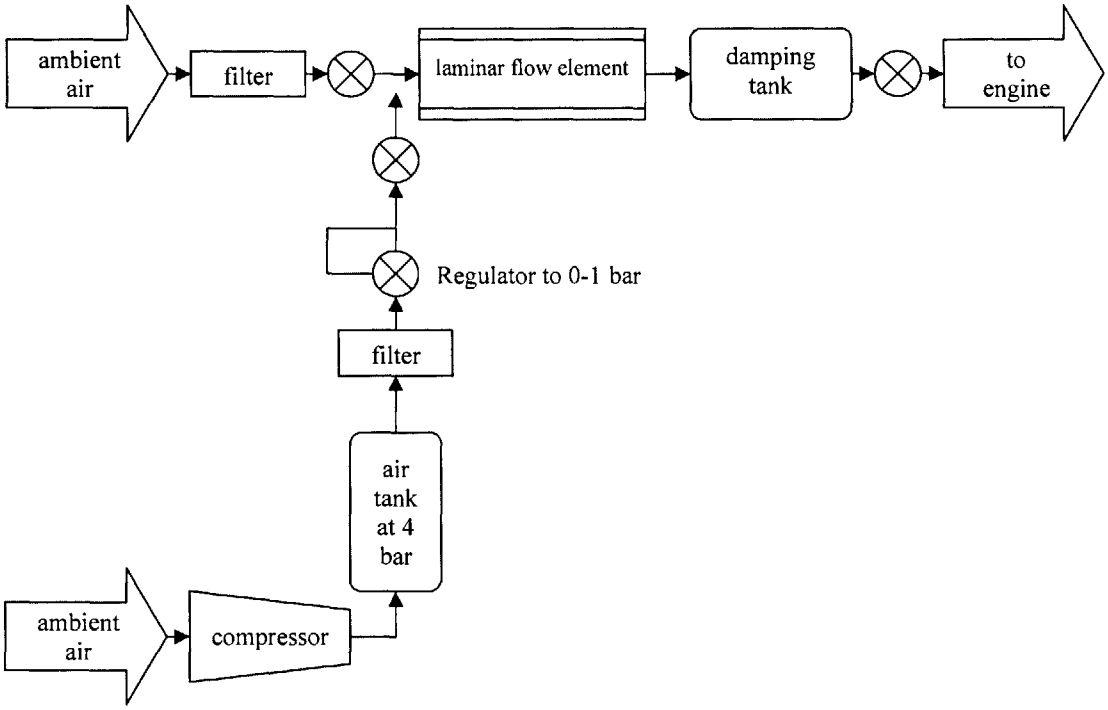

Figure 2. 1: Diagram of Air Intake System

Fuel entered the system from an interchangeable fuel tank. It was pumped from this tank to the engine through a filter. As the fuel reached the engine, there was a regulator which ensured that the fuel line pressure was maintained at a constant differential pressure (~3 bar) from the average intake manifold pressure. The regulator also returned any excess fuel not injected for the cycle to the fuel tank. When switching between fuels, the system was purged using a nitrogen gas stream. This nitrogen purge allowed for the removal of all fuel from the system, except for the small volumes in the accumulator, regulator, and

injector supply line. The system also allowed fuel to be sent to a slop tank to avoid contamination of the main tank. Figure 2. 2 shows a schematic of the fuel intake system.

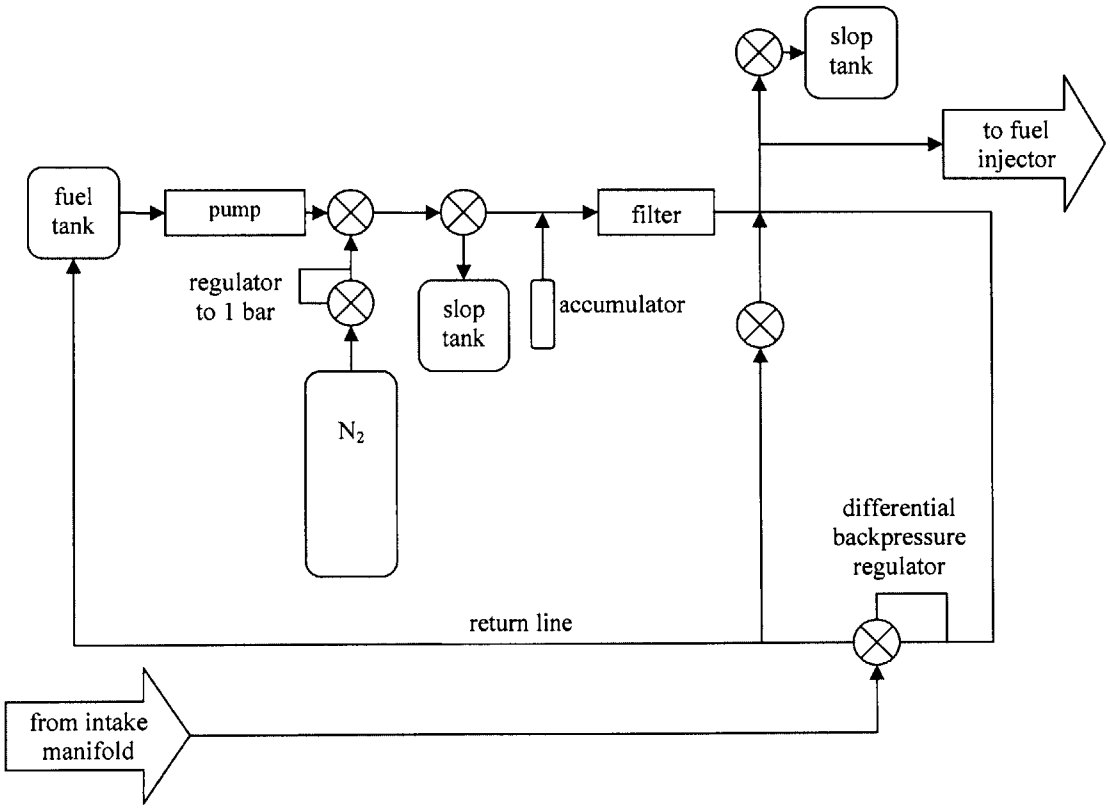

Figure 2. 2: Diagram of Fuel Intake System

2.2 ENGINE CONTROL AND MEASUREMENTS

This section describes the control and measurement systems in place for this test cell.

2.2.1 Engine Control Unit

The engine control unit (ECU) for this set-up was a MoTeC M4 engine controller and was used to control the fuel injector and ignition system. The injection timing was set for 385° BTC with a dwell of 4 ms. The ECU allowed for adjustment to the injector pulse width and spark timing as the engine was running.

2.2.2 Intake Pressure Control and Measurement

The manifold pressure was controlled by manually adjusting a throttle valve from outside the test cell through the use of a stepper motor. Pressure transducers measuring absolute pressure were used to measure intake pressure at two locations. The first location, which measured the pressure of the air damping tank, was between the air flow meter and the throttle plate. The second location, which was used to measure manifold absolute pressure (MAP), was between the throttle plate and the engine. Both measurements had digital readouts to display the results.

2.2.3 Temperature Control and Measurement

The temperatures of engine coolant and engine oil were controlled. The engine coolant temperature was maintained between 90 °C and 95 °C by an electric heater/electronic thermostat and cold water heat exchanger/mechanical thermostat combination. The oil temperature was maintained between 70 °C and 80 °C by an electric heater/electronic thermostat. The engine had four temperature measurement locations including the engine coolant inlet, the intake air in the tank between the flow meter and the throttle plate, the engine oil inlet, and the engine exhaust approximately 2 cm from the exhaust port outlet.

2.2.4 Air Flow Measurement

The volumetric flow rate of air was determined with the use of a differential pressure sensor across a laminar flow element. The volumetric flow rate was then converted to a mass flow rate using the ideal gas law as well as the air tank pressure and temperature measurements. A humidity measurement was used to correct the air mass flow rate for water content. The accuracy of the air mass flow rate was approximately ±2%.

2.2.5 Fuel Flow Measurement

The fuel injector pulse width was used for determining the amount of fuel injected during each cycle. This method allows for fast measurements with an accuracy of roughly ±2%. As mentioned earlier, the fuel pressure regulator maintains a constant differential between the average intake manifold pressure and the fuel injector supply line pressure. When the injector is open there is a constant flow through the injector orifice. Using a previously completed experimental calibration, the injector pulse width can be used to calculate the mass of injected fuel. The limitations in accuracy for this method are due to

pressure variations across the injector caused by high-speed fluctuations in the intake manifold pressure as well as effects caused by variations in fuel density caused by temperature variations.

2.2.6 Air-Fuel Ratio Measurement

A Universal Exhaust Gas Oxygen (UEGO) sensor was used to measure exhaust gas oxygen content. The UEGO reading was then converted to an air-fuel equivalence ratio or lambda reading with the use of a Horiba Mexa-110λ analyzer.

2.2.7 Cylinder Pressure Measurement

Cylinder pressure was measured using a Kistler 6125A piezoelectric pressure transducer with a flame arrestor. The current signal from this pressure transducer was converted to a voltage signal with the use of a charge amplifier. This voltage signal was then collected at a rate of approximately ten times per crank angle degree using a National Instruments 6023E data acquisition card triggered by a BEI crankshaft encoder. A program written in National Instruments LabVIEW recorded 100 cycles of cylinder pressure data when triggered.

This cylinder pressure data in combination with a version of Sloan Automotive Laboratory's burn rate analysis software, modified for use with high acquisition speed data, was used to calculate:

- Peak pressure
- Crank angle of peak pressure
- 0-10% mass fraction burned time
- 0-50% mass fraction burned time
- 10-90% mass fraction burned time
- Net Indicated Mean Effective Pressure (NIMEP)

2.2.8 Knock Detection

A microphoned audible knock method was used to detect knock onset. A microphone hung ~1/4 inch above the valve cover of the engine. This microphone was connected to an equalizer set to remove all frequencies except those near 6 kHz and 12 kHz. The

audio signal was then passed to a set of headphones where the operator could listen to the signal in order to detect knocking conditions.

This knock detection method was chosen because it was shown effective in previous work [9] and because it avoided the complexity of a sensor-based knock detection system. It can be roughly estimated that microphone knock occurs at a spark timing 2 crank angle degrees more retarded than knock that can be detected by the naked ear. This method is somewhat subjective, but on average, between two different operators, the knock limit is agreed upon within two octane numbers or 2 crank angle degrees.

2.2.9 Microphone Measurement

The National Instruments LabVIEW software was also set up to record the signal heard by the microphone. One hundred cycles of the microphone signal could be recorded simultaneously with the cylinder pressure data.

2.3 EXPERIMENTAL PROCEDURES AND INFORMATION

Tests were completed to collect data that could be analyzed in order to gain a better understand the knock onset phenomena.

2.3.1 Experimental Procedure

Before beginning any experiments, both the dynamometer and engine were fully warmed up. Below is a list of the steps taken in order to complete a spark timing sweep. Experimental results were recorded in a spreadsheet which was used to calculate burn angles and other relevant parameters.

1. Set the engine speed with the dynamometer controller.
2. Position the throttle plate to the wide-open position.
3. Make an initial estimate of the maximum brake torque (MBT) timing from previous trends.
4. Adjust the fuel injector pulse width using the MoTeC ECU until a stoichiometric air-fuel ratio is achieved.
5. Using the microphone and headphones, find the spark timing at which knock onset occurs. Advance the spark timing by 3° CA.

6. Record operating conditions and cylinder pressure data.
7. Retard the spark timing in increments of 1° CA, repeating Step 6 for each increment until the spark timing is 3° CA more retarded than the knock onset timing. While retarding the spark timing, minor adjustments to the throttle position may need to be made in order to maintain a stoichiometric exhaust air-fuel ratio. Care should be taken to avoid exceeding the maximum cylinder pressure of 110 bar, an exhaust temperature greater than 750° C, or any extreme knocking condition that might lead to engine damage.

2.3.2 Experimental Fuels

Toluene reference fuels (TRF) were used for all experiments. It was felt that TRFs better represented the sensitivity and aromatic content of gasoline than did primary reference fuels (PRF). TRFs are a mixture of toluene and n-heptane while PRFs are a mixture of iso-octane and n-heptane. Figure 2. 3 shows the research octane number (RON) and motor octane number (MON) for several TRFs plotted as a function of the volume fraction of n-heptane. The fuels used for this research had research octane numbers that ranged between 85 and 100 in increments of 5.

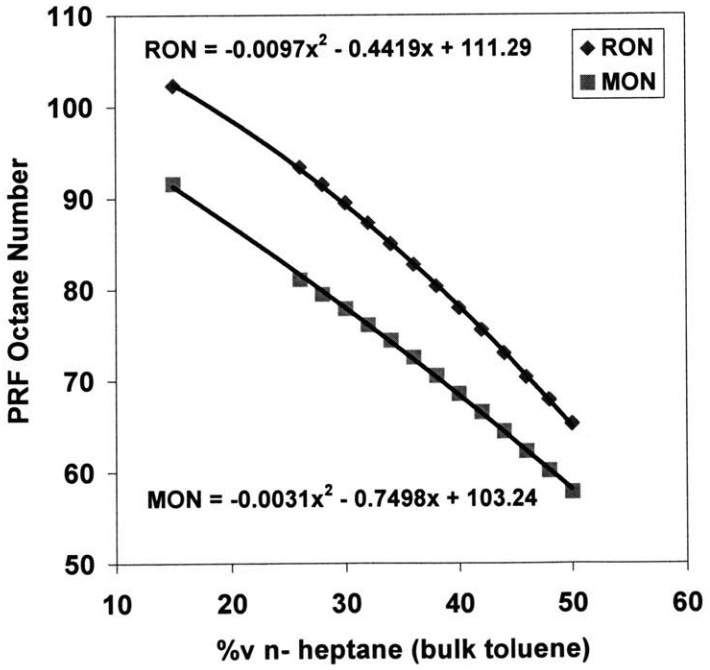

Figure 2. 3: RON and MON of TRFs, (Taken from Gerty [10], courtesy of Shell Global Solutions)

(page intentionally left blank)

CHAPTER 3: DATA AND DATA PROCESSING METHODS

3.1 DATA SETS

All cylinder pressure and microphone data were acquired at a high acquisition speed of 90 kHz, which at an engine speed of 1500 RPM is equivalent to 10 samples per crank angle degree. Data acquisition was triggered for every cycle by the BDC signal. Previously, most cylinder pressure data had been obtained using a lower sampling frequency of only 1 sample per crank angle degree. It was determined, however, that this slower sampling rate did not allow for an adequate observation of the more subtle behaviors of the cylinder pressure during conditions of engine knock.

3.1.1 Experimental Conditions

All data discussed here was taken on one of two days. Table 3. 1 shows the engine operating parameters used during testing. The only differences in conditions between the two test days were the laboratory air temperature and relative humidity. For the data taken in July, the air temperature was 99 °F with a relative humidity of 23%. The air temperature for the data taken in March was 83 °F with a relative humidity of 9.5%. Due to the change in atmospheric conditions some of the knock onset timings were slightly different for the different days. These differences can be found in Table 3. 2 and Table 3. 3.

Table 3. 1: Engine Operating Parameters

Compression Ratio	9.8:1
Speed (RPM)	1500
Lambda	1.0
MAP (bar)	1.0
MBT Spark (°BTC)	~17

Table 3. 2: Spark Timings for Data Taken on July 26, 2005

Level of knock/fuel type (timings in °BTC)	TRF85	TRF90	TRF95	TRF100
non-knocking	-6	-4	2	5
	-5	-3	3	6
	-4	-2	4	7
knock onset	-3	-1	5	8
	-2	0	6	9
	-1	+1	7	10
heaviest knock	0	+2	8	11

Table 3. 3: Spark Timings for Data Taken on March 23, 2006

Level of knock/fuel type (timings in °BTC)	TRF85	TRF90	TRF95	TRF100
non-knocking	-7	-5	0	5
	-6	-4	1	6
	-5	-3	2	7
knock onset	-4	-2	3	8
	-3	-1	4	9
	-2	0	5	10
heaviest knock	-1	+1	6	11

3.1.2 Filter Parameters

All filters used were created using MATLAB's *Filter and Design Analysis* tool. This toolbox is a user interface that easily allows the user to input all of the necessary filter parameters including filter type, design method, order, frequency specifications, and magnitude specifications. The tool then designs the filter and the filter coefficients can be exported to a text file to be used in combination with a filter command in a MATLAB program.

All filters were finite impulse response equiripple bandpass filters with a minimum order and density factor of 16. The magnitude specifications were 60 dB for the first stop, 1dB for the pass, and 80 dB for the second stop. The frequency specifications for all of the filters discussed in this text can be found in Table 3. 4.

Table 3. 4: Frequency Specifications for All Filters

Frequency Range (all units in kHz)	**6-7**	**15-20**	**6-23**
sampling frequency	90	90	90
first stop	5	14	5
first pass	6	15	6
second pass	7	20	23
second stop	8	21	24

When filtering data, MATLAB's filtfilt command was used. This command was chosen because it filters the data in the forward direction, reverses the filtered sequence, and runs it back through the filter. In doing so, any phase shift induced from the act of filtering the data is removed. It was important to avoid a phase shift in the data in order to accurately determine the crank angle of knock onset. The use of the filtfilt command also removed most of the drift away from zero that was seen in many traces.

3.1.3 Smoothing Technique

A smoothing technique was used in creating the mean removed pressure traces. The pressure trace was divided up into 20-point segments. These 20 points were averaged to create a pressure trace consisting of only 360 points. These 360 points were then taken and expanded back out to 7200 points by interpolating between each point. This was done to create a smooth, average pressure trace. This smoothed pressure trace was then subtracted from the original 7200 points in order to generate the mean removed pressure traces.

This allowed for the pressure trace to be flattened and made studying the oscillations and subtleties of the pressure trace much easier without the distraction of the underlying

pressure trace and extraneous signal noise. The one difficulty with this method is choosing an appropriate number of points to use for the subsets. When using 20 points, much of the extraneous noise in the pressure trace is removed; however, just before the point where the oscillation amplitudes quickly begin to rise, there is often a large dip. This dip is created due to averaging points that are usually very rapidly increasing from the beginning of combustion. Using a large subset of points makes this rapid increase more obvious over a larger number of points when the interpolation is done to expand back to 7200 points. When these artificially higher numbers are subtracted back out from the original trace, a dip is created. This dip can be avoided by using a much smaller number of points for the subset, such as 4. The problem with using a subset as small as 4 is that the subsets are too small to remove a great deal of the extraneous signal noise making the traces once again difficult to interpret. An intermediate subset value of 10 is sufficient to remove most of the extraneous signal noise but does little to affect the presence of the dip; therefore, a subset value of 20 was used in order to remove as much signal noise as possible.

3.1.4 Microphone Signal Processing

Towards the end of experimentation, a small amount of microphone data was recorded simultaneously with the cylinder pressure trace data to allow for comparison. The same microphone, sound equipment, and set-up used for listening to the engine through headphones to determine knock was used in recording this data. Because the single microphone signal was simultaneously used to determine knock onset and record data, the equalizer was still used and filtered the signal for all signals except those around 6 kHz and 12 kHz. It should also be noted that the volume setting on the microphone affected the magnitude of the microphone signal recorded. The volume level was held constant for all data sets taken with TRF85, 90, and 95 fuels, however, due to the fact that knock becomes more difficult to audibly detect at higher octane values, it was necessary to increase the volume for the TRF100 fuel in order to determine the spark timing of knock onset.

3.2 DATA PROCESSING AND ANALYZATION

This section contains a summary of the successful data processing and analysis methods found throughout this research.

3.2.1 Determining the Cylinder Pressure Signal Frequencies

Power spectrum analyses were done for several different sets of data to confirm the proper frequency ranges to use in filtering the cylinder pressure data. This analysis was completed using MATLAB's fft command. Figure 3. 1, Figure 3. 2, and Figure 3. 3 display representative samples of power spectra for non-knocking, at knock onset, and heavier knocking situations with a TRF95 fuel. It is easily seen that there are three prevalent frequency bands in the pressure signal. The first band is at 6.5 kHz, the second at approximately 9 kHz, and the last around 17.5 kHz. Care should be taken when examining these plots to note the differences in the y-axis values which represent the power density of particular frequencies occurring in a data set.

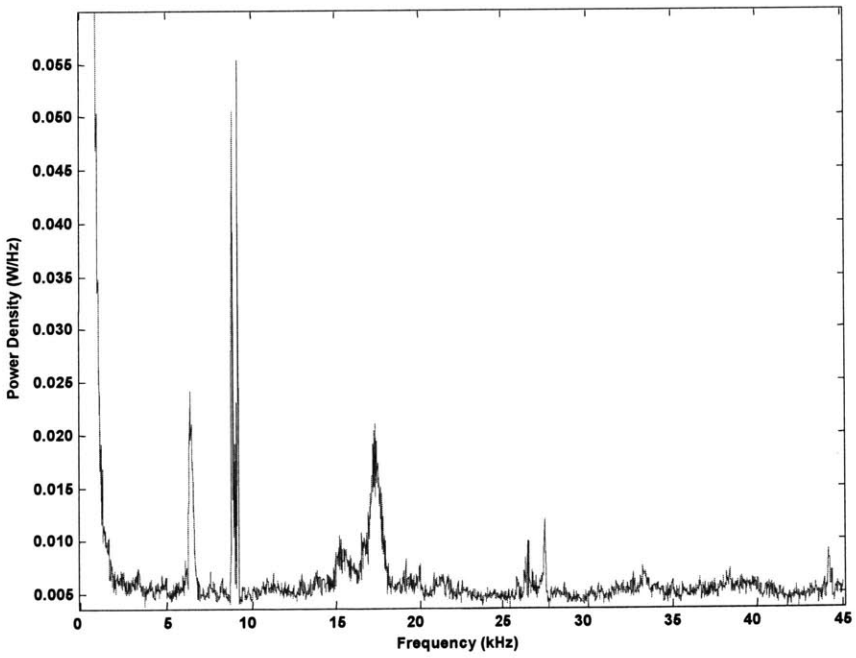

Figure 3. 1: Power Spectrum for Non-Knocking Data

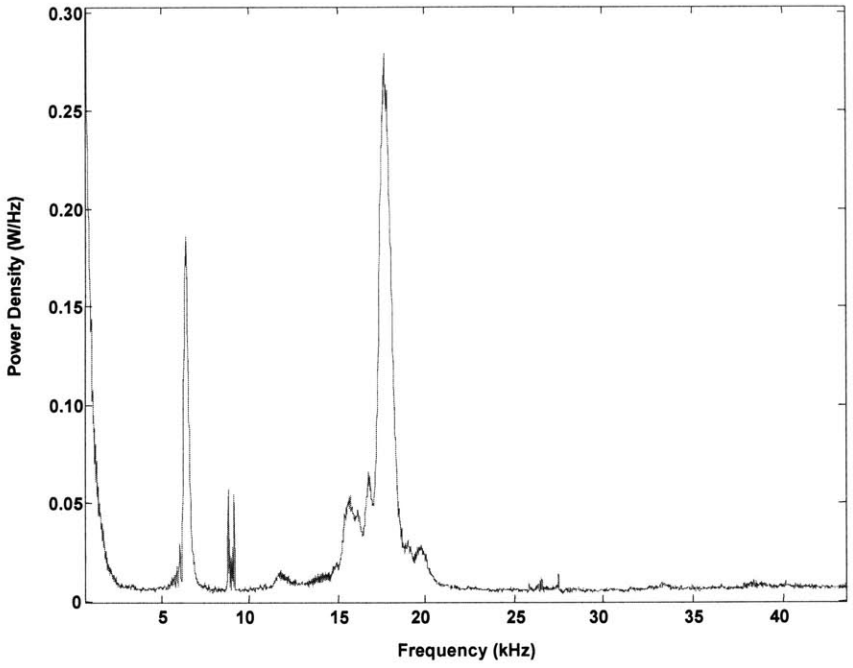

Figure 3. 2: Power Spectrum for Knock Onset Data

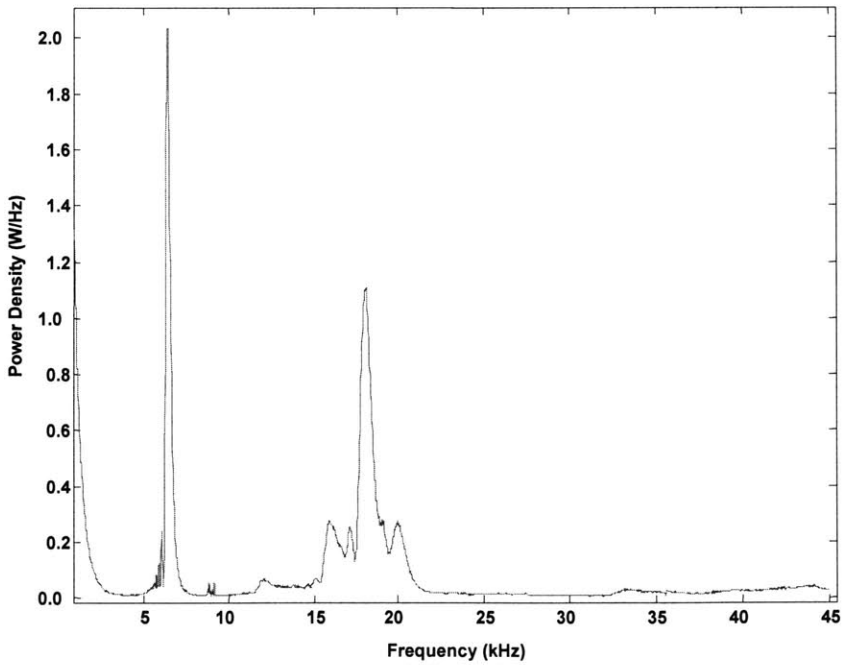

Figure 3. 3: Power Spectrum for Heavy Knocking Data

For data sets that are non-knocking (Figure 3. 1), the second band shows the most prevalence, with the first and third showing considerably smaller power densities. Progressing to the knock onset power spectrum (Figure 3. 2), the power density of the second band maintains the same numeric power density value, but there is a dramatic increase in the power density for both the first and third bands. A nearly ten-fold increase in the first band and an over ten-fold increase in the third band are observed. It is not always the case, that the third band shows a greater prominence than the first.

Continuing on to a higher level of knock (Figure 3. 3), again the power density value of the second band remains constant while the first and third again increase drastically. This time the first band increased another ten-fold while the third band only quadrupled. These power spectra analyses show that more than a single signal or pressure wave frequency exists throughout an entire engine cycle. It does not, however, provide any information as to where or when these frequencies might exist.

3.2.2 Knock Indications in Filtered Cylinder Pressure Signal

It has been determined that cycles with autoignition events that lead to engine knock display certain characteristics. These characteristics are the knock intensity of a cycle compared to the number of oscillations required to reach the maximum amplitude on a band pass filtered pressure trace. Throughout this work, knock intensity (KI) is defined as the difference between the maximum pressure and the minimum pressure of the 6-7 kHz bandpass filtered pressure trace. This method compensates for pressure traces that might have some drift and are not perfectly centered around zero. This drift usually only occurs for cycles with very low KI. It should also be noted that in using this definition, every single cycle, regardless of its level of knock, will have a KI value because every single cycle will have a maximum and minimum on the bandpass filtered pressure trace.

Figure 3. 4 and Figure 3. 5 show filtered pressure traces with markings describing the points used for calculating KI. These figures also illustrate how the number of oscillations required to reach the maximum amplitude is calculated. The initial "blip" that exists at the beginning of many of the bandpass filtered pressure traces is ignored. At the time of writing, it has not been established if the presence of this "blip" is created

by the filtering method or has a physical meaning. The count for oscillations begins immediately after this "blip" or at the lowest amplitude point before the build-up. The oscillations are counted by the top of each oscillation until the peak amplitude has been reached.

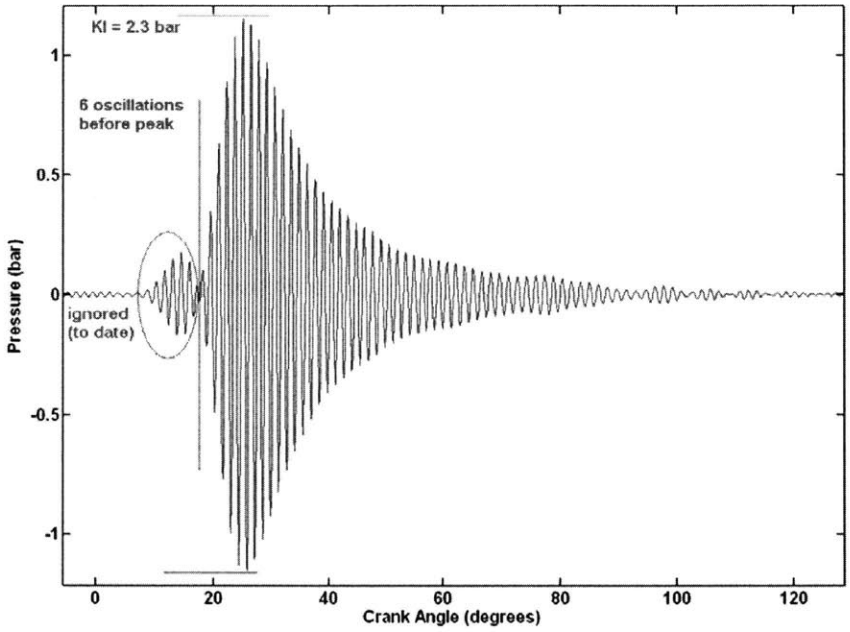

Figure 3. 4: Low Oscillation Knock Intensity Figure (TRF95, 7°BTC)

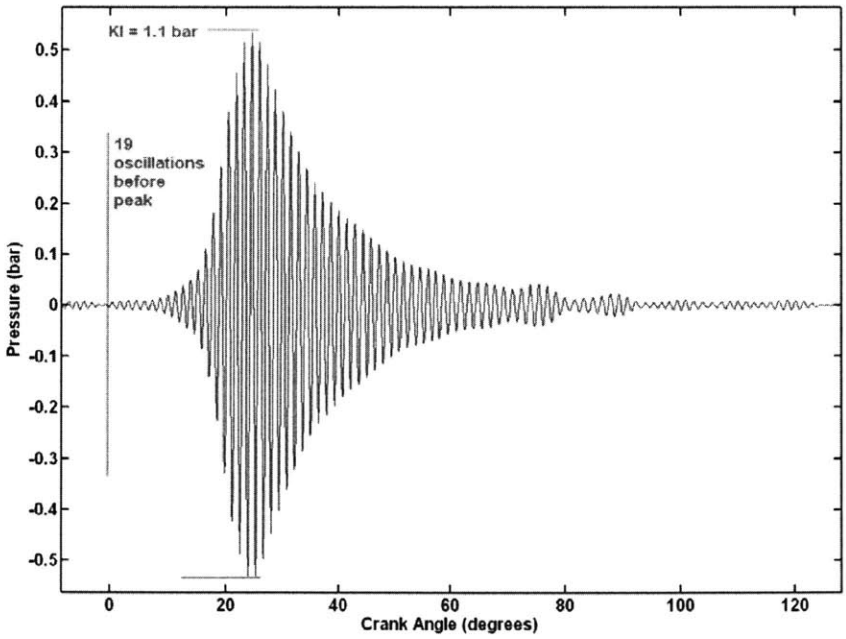

Figure 3. 5: High Oscillation Knock Intensity Figure (TRF95, 7°BTC)

The KI and number of oscillations required to reach the maximum amplitude can then be plotted on a cycle by cycle basis. The first example of this is Figure 3. 6 which shows data for a TRF95 fuel with non-knocking spark timings as well as the knock onset spark timing. The knock onset spark timing is represented by the triangles. This plot shows that for the three non-knocking spark timings nearly all of the cycles have KI values below 1 bar, and there is a scattering in the number of oscillations before peak. However, when the spark timing of knock onset is reached, a few points enter the region of KI greater than 1 bar and have a range of 5-10 oscillations before peak.

Figure 3. 7 then shows spark timings that produce higher levels of knock while still displaying the sparking timing of knock onset as triangles. This figure shows that as heavier knock is induced an increased number of points proliferate the region where KI is greater than 1 bar with 5-10 oscillations before peak. The presence of points in this specific region of these plots is one useful method in detecting knock onset. Similar figures to Figure 3. 6 and Figure 3. 7 but with different octane ratings can be found in the appendix. Figure 3. 8 also provides an overview of what can be found in the appendix by displaying the percentage of cycles in particular oscillation ranges that have KI greater than 1 bar. The arrow in each plot points to the spark timing of knock onset. It can be seen that in all four plots at the spark timing of knock onset cycles with 5-10 oscillations begin to appear for all octane ratings.

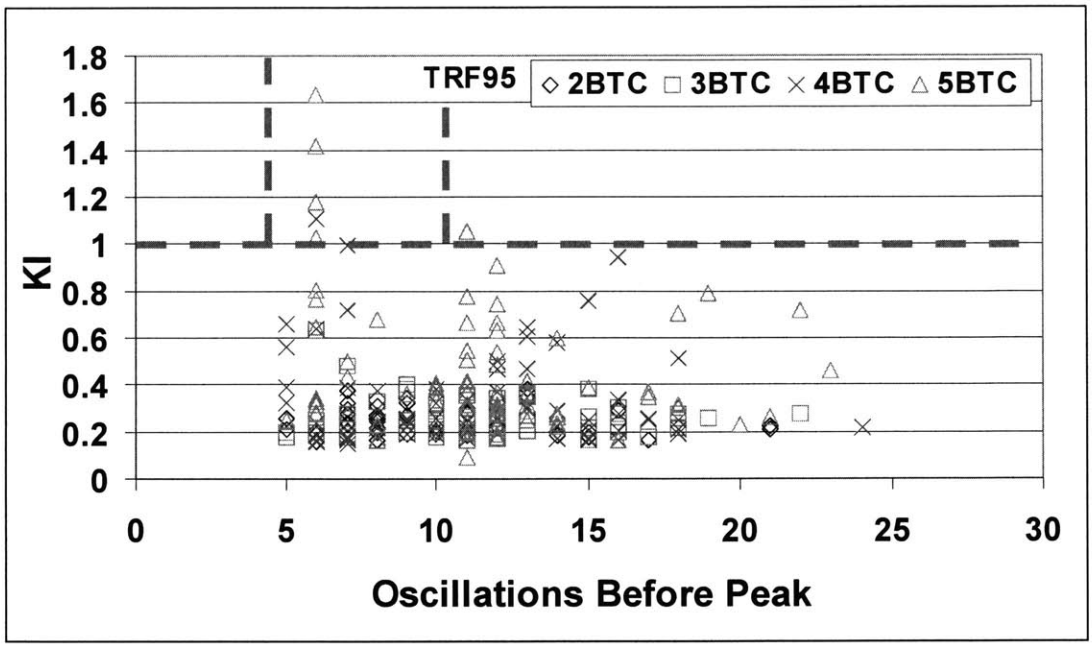

Figure 3. 6: Non-Knocking and Knock Onset Spark Timings for Relationship of Number of Oscillations with KI

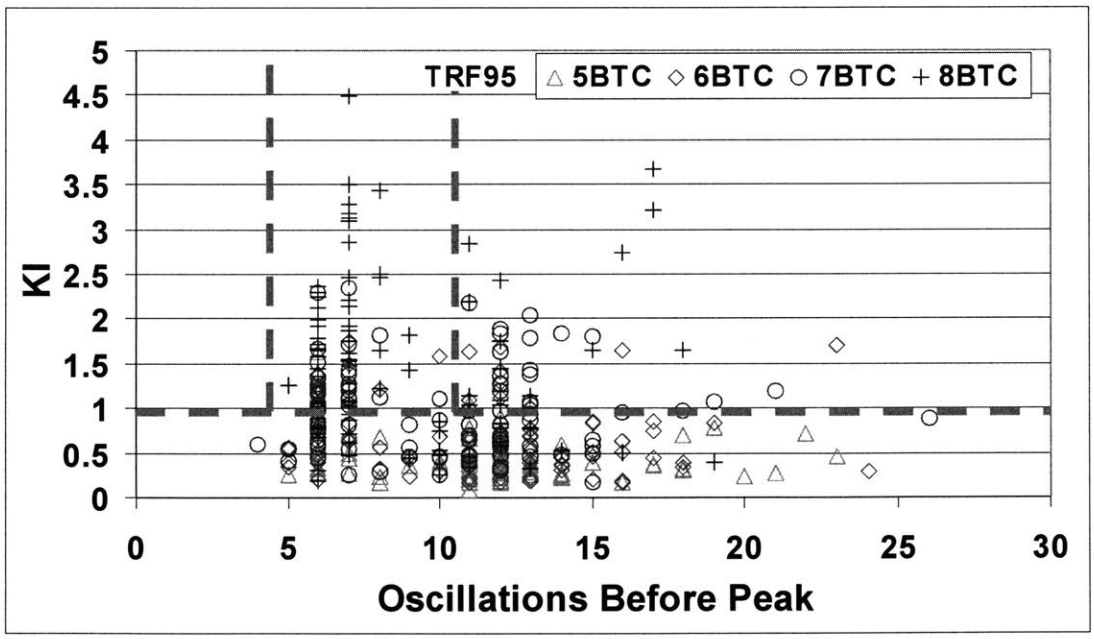

Figure 3. 7: Knock Onset and Heavier Knocking Spark Timings for Relationship of Number of Oscillations with KI

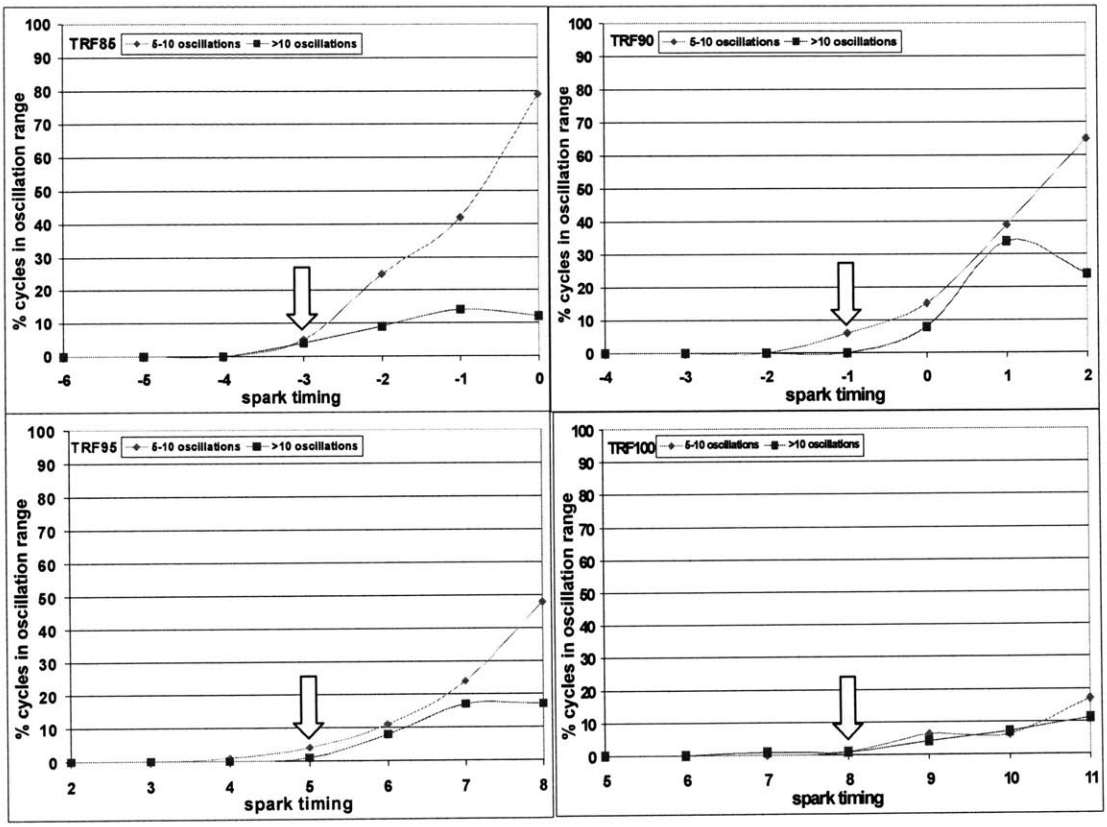

Figure 3. 8: Trends in the Number of Oscillations for all Four Fuel Types

The information provided in these plots can also be used to develop insight into what may be taking place inside the cylinder during engine knock. The low number of oscillations before peak indicates a rapid build-up of the pressure wave. A rapid sequential autoignition of more than one center could cause and maintain these significant amplitude pressure waves. These plots, however, do not provide any insight as to why such a modest number of higher amplitude waves can cause strong enough block and head vibrations to create an audible noise outside the engine.

Another trend in the data is seen by plotting the knock intensity versus the $(dP/d\theta)_{max}$ which can be seen in Figure 3. 9. This trend shows a similar transition behavior at knock onset as that from plotting the number of oscillations before peak. As knock level increases, the number of points at higher KI and higher $(dP/d\theta)_{max}$ levels increases. More important is the trend seen in the average of these values over all the cycles. A plot of the

average values for all spark timings can be found in Figure 3. 10. With all four fuels tested, it was seen that at knock onset the average KI value was approximately 0.4 bar and the average $(dP/d\theta)_{max}$ value was approximately 10 bar/°CA. This could be a useful calculation in determining knock onset without an operator. Further plots for fuels of varying octane ratings can be found in the appendix to confirm both these trends.

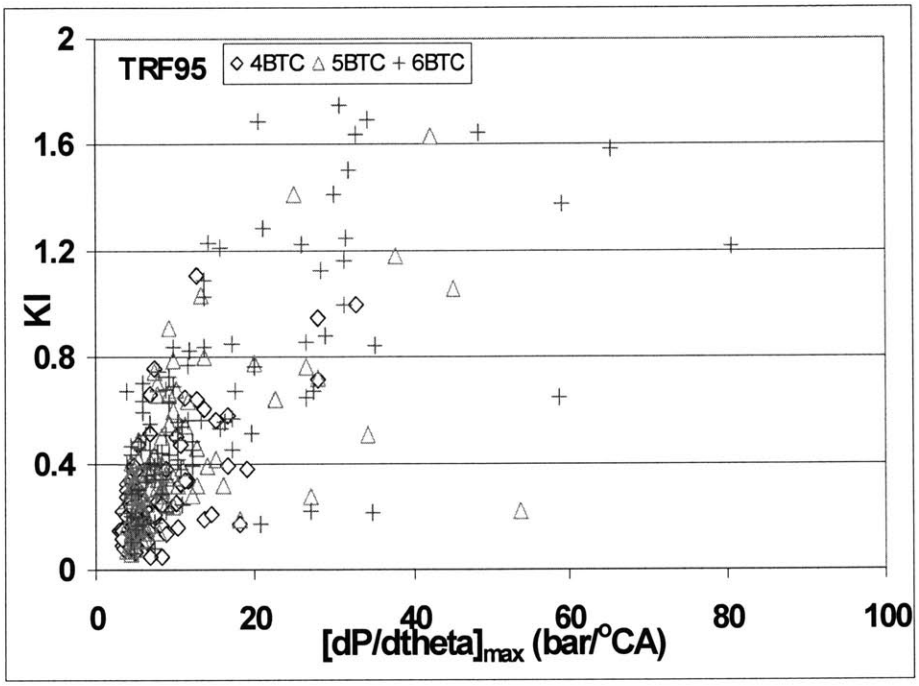

Figure 3. 9: Transition of Points to Higher KI and $(dP/d\theta)_{max}$ values at Spark Timings Before, At, and After Knock Onset

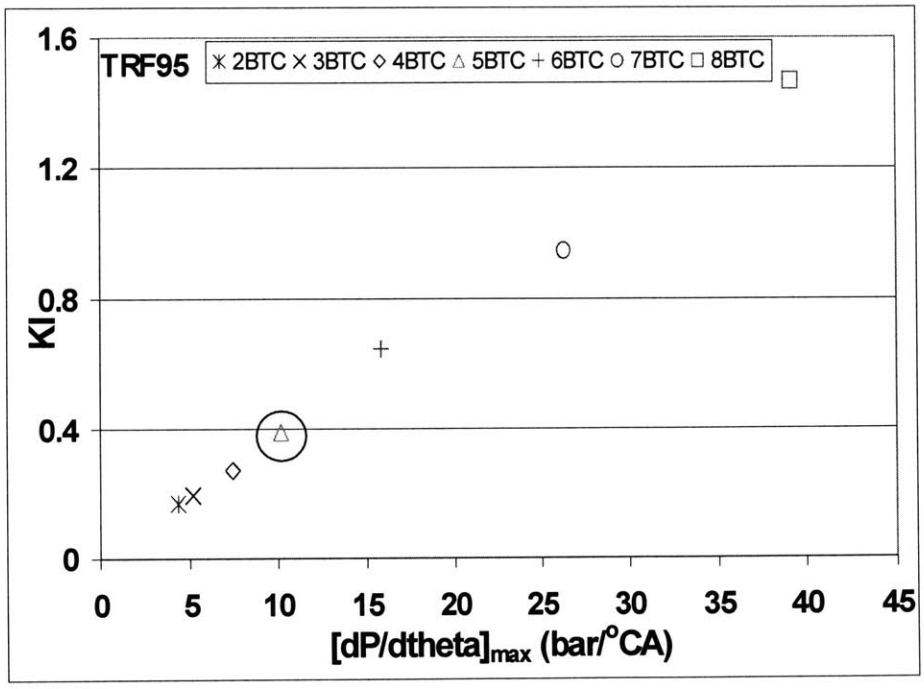

Figure 3. 10: Key Location of Knock Onset Averages

Figure 3. 11 now highlights those critical cycles from the plots of KI versus the number of oscillations to reach maximum that are in the region of KI greater than 1 bar and have 5-10 oscillations before peak on the plots of KI versus $(dP/d\Theta)_{max}$. These critical cycles are represented by solid triangles. This figure shows a relationship between the critical cycles from the oscillation plots, higher knock intensities, and higher $(dP/d\Theta)_{max}$ at knock onset. Again, similar plots but with varying octane rated fuels can be found in the appendix.

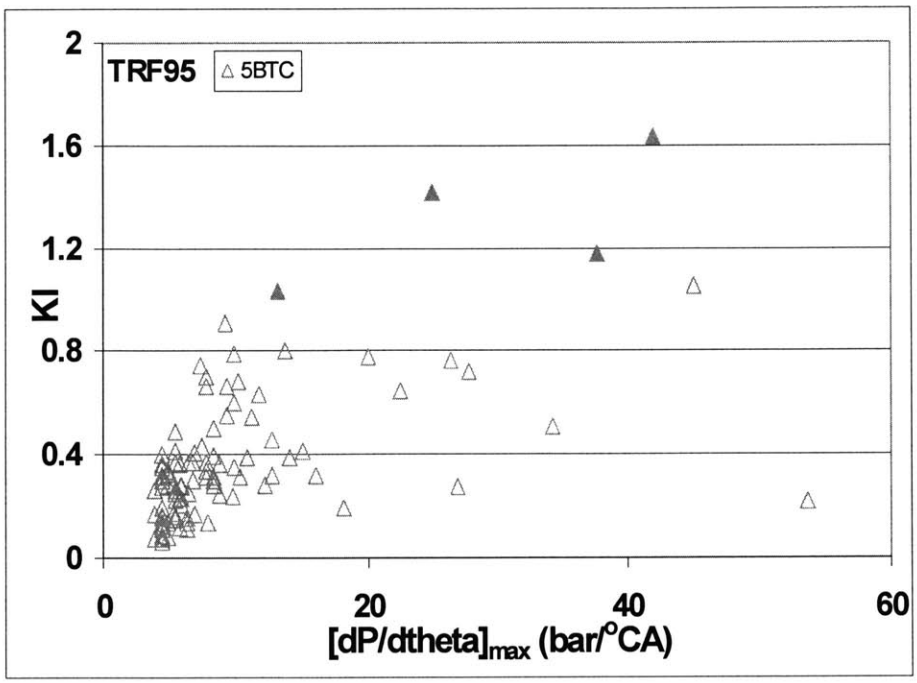

Figure 3. 11: Highlight of Points with KI > 1 bar and 5-10 Oscillations Before Peak

3.2.3 Data Analysis Method for Cylinder Pressure without Filtering

Figure 3. 12, Figure 3. 13, and Figure 3. 15 show three-tier magnified plots relating the raw pressure trace (top), 6-7 kHz bandpass filtered pressure trace (middle), and mean removed pressure trace (bottom). The range for the bandpass filtered pressure trace was chosen as it is the first resonant frequency of knock for this engine. Its presence also becomes more and more significant as the level of knock increases.

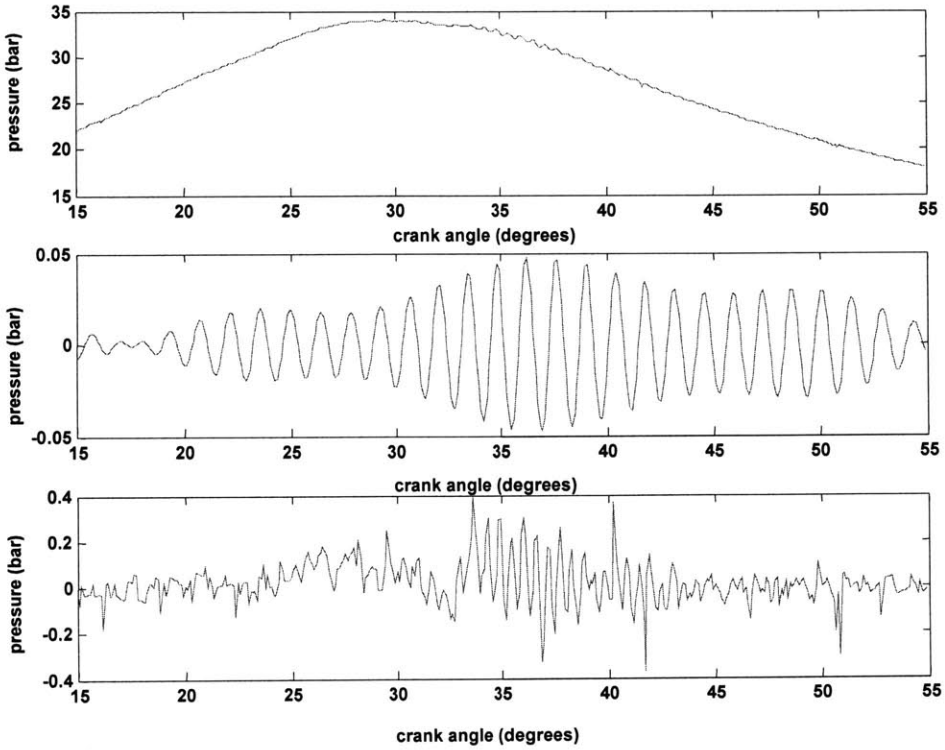

Figure 3. 12: Three-Tier Magnified Plot for a Representative Non-Knocking Spark Timing of 0° BTC, KI~0.1 bar (Raw Pressure Trace (top), 6-7 kHz Bandpass Filtered Pressure Trace (middle), and Mean Removed Pressure Trace (bottom))

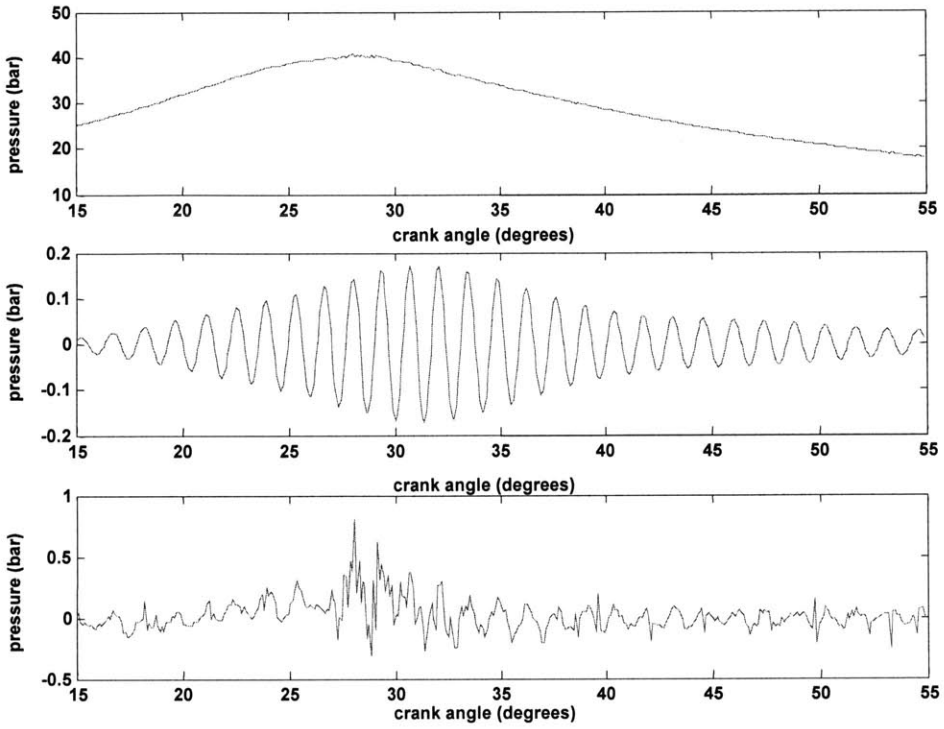

Figure 3. 13: Three-Tier Magnified Plot for a Representative Knock Onset Spark Timing of 3° BTC, KI~0.4 bar, 14 oscillations (Raw Pressure Trace (top), 6-7 kHz Bandpass Filtered Pressure Trace (middle), and Mean Removed Pressure Trace (bottom))

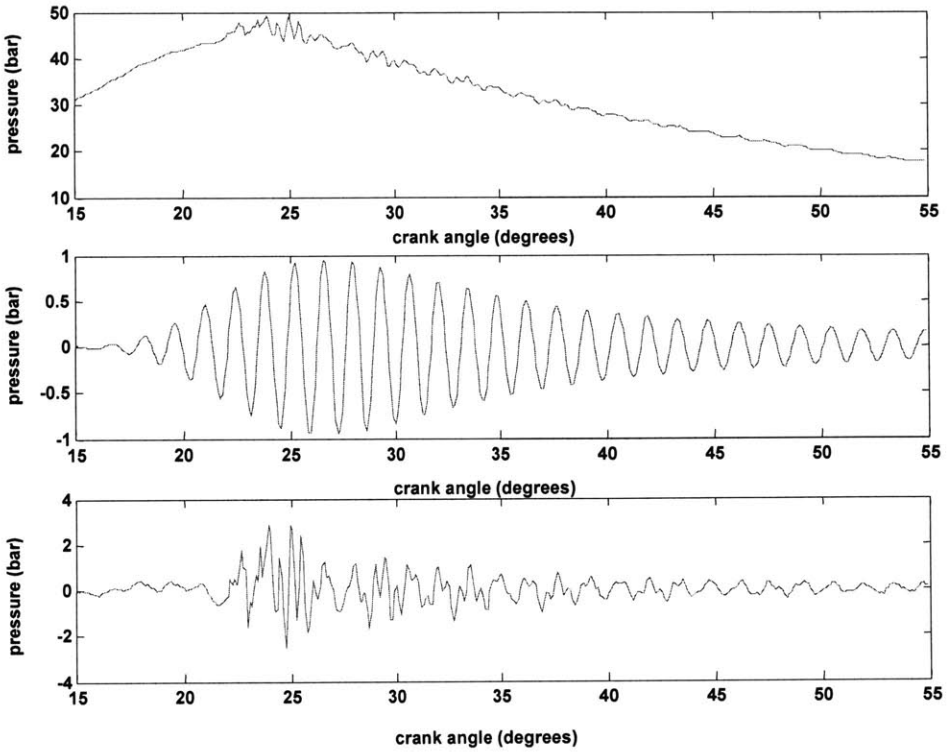

Figure 3. 14: Three-Tier Magnified Plot for a Representative Knock Onset Spark Timing of 3° BTC, KI~2bar, 7 oscillations (Raw Pressure Trace (top), 6-7 kHz Bandpass Filtered Pressure Trace (middle), and Mean Removed Pressure Trace (bottom))

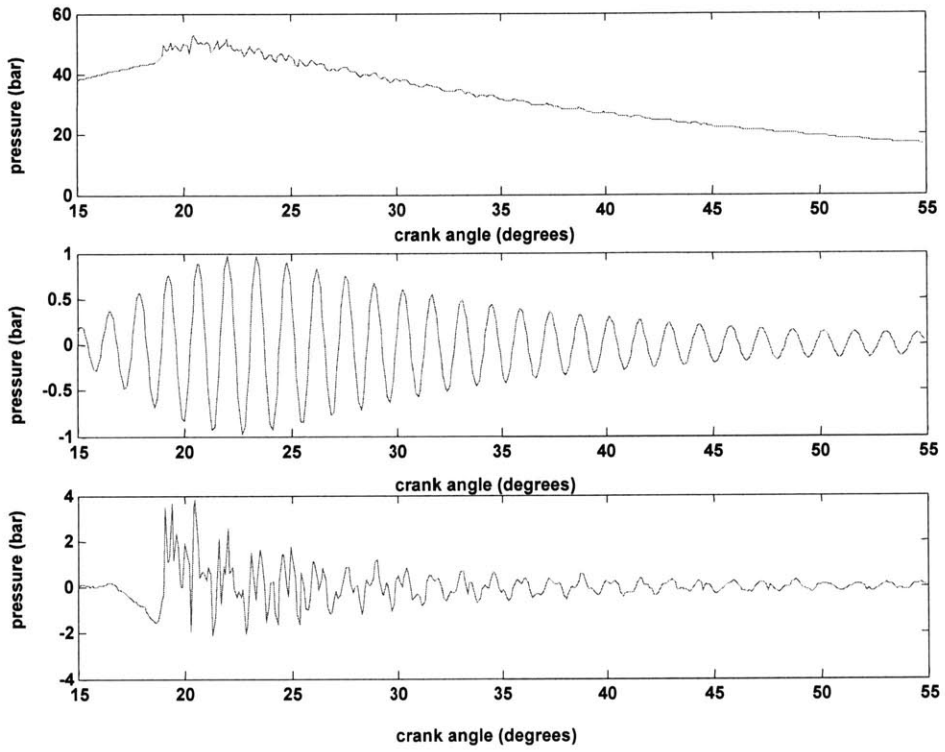

Figure 3. 15: Three-Tier Magnified Plot for a Heavily Knocking Spark Timing of 6° BTC, KI~2 bar, 7 oscillations (Raw Pressure Trace (top), Bandpass Filtered Pressure Trace (middle), and Mean Removed Pressure Trace (bottom))

In using the three-tier plots, it was revealed that the 6-7 kHz bandpass filtered pressure trace shows an autoignition initiation earlier than that expected from either the raw pressure trace or the mean removed pressure trace. Additionally, in the mean removed pressure trace plots, the presence of multiple frequency bands was highlighted. Along with the presence of multiple frequency bands, the mean removed pressure traces outline rough regions where certain frequencies exist. In cycles that obviously exhibit characteristics of autoignition that lead to engine knock, such as that in Figure 3. 15, there is a strong prevalence of the 6.5 kHz signal from the crank angle of knock onset and continuing on through the pressure trace. In addition to this lower frequency signal, there is an overlay of higher level frequencies on top of the lower frequency. High frequency signals exist throughout the entire pressure traces, but their amplitude rises sharply in the region immediately following the crank angle of knock onset. These higher level

frequencies, however, fade after a short period of time down to only the 6.5 kHz signal. The number of crank angles it takes for the higher level frequencies to die down is shorter for cycles that lead to heavier engine knock.

The initiation of the multiple frequency oscillations in the mean removed pressure trace usually coincides quite well with the initiation of the rise in amplitude of the band pass filtered signal. In cycles that do not have autoignition events that lead to engine knock such as those in Figure 3. 12, the higher level frequencies often still have a sharp rise near the same point where the amplitude in the band pass filtered signal also rises, but in these non-knocking cycles, the higher level frequencies do not fade into a 6.5 kHz signal but maintain a higher frequency throughout. With cycles that have autoignition events that lead to heavier engine knock, the higher level frequencies fade into an even smoother and more regular 6.5 kHz signal.

A pseudo knock intensity can be determined for the mean removed pressure traces by subtracting the minimum pressure from the maximum pressure. When using this particular method with this adjusted pressure trace, there is no guarantee that the maximums and minimums will be very close to each other, hence, the use of the word pseudo knock intensity. This is due to the multiple frequencies seen from using the three-tier plots. At the extreme non-knocking and heavy knocking ends, the pseudo knock intensity has a relatively clear trend. It shows that very small pseudo knock intensities mean the cycle did not contain an autoignition event leading to engine knock and very large pseudo knock intensities mean the cycle did contain an autoignition event leading to engine knock. This trend is not accurate with mid-range pseudo knock intensities and the status of the cycle could lean towards either non-knocking or knocking; therefore, a pseudo knock intensity cannot be used to determine engine knock without additional information.

All of the information just presented can be combined in order to show a progression through the transition from non-knocking conditions to heavily knocking conditions. For non-knocking conditions, on a mean removed pressure trace, there is no distinct jump in

the pseudo knock intensity level showing an autoignition initiation point. This trace does not have any areas with distinct frequencies. The entire trace appears to be full of noise. As the knock onset point is approached, a few cycles will begin to have characteristics more like those seen in the knock onset cycles including higher jumps in pseudo knock intensity level. With the exception of a few random cycles that are not able to maintain engine and head vibrations strong enough to create an audible knock event, these cycles do not contain the 6.5 kHz signal late in the trace that appears at the knock onset point.

At knock onset, using the mean removed pressure traces, an autoignition initiation point can be identified where there is a sudden jump in the pseudo knock intensity level. At this point, there is also the presence of more than one frequency in the signal for a short period of time, roughly 5-10 crank angle degrees. This period of multiple frequencies quickly fades to a signal that only contains the 6.5 kHz frequency after a short period of time in those cycles that contain autoignition events that lead to engine knock. Depending on the octane rating of the fuel used, the percentage of cycles that behave in this manner at the knock onset conditions ranges from 5-50%. Those cycles that do not show autoignition events that lead to engine knock either look like those described in the paragraph above regarding non-knocking cycles or have an appearance somewhere between these two descriptions. These cycles will still contain the multiple frequencies for a short period of time with a less distinct beginning, but will not fade into a clear 6.5 kHz signal. The presence of higher order frequencies persists.

For heavier knocking conditions, on a mean removed pressure trace, the sudden jump in the pseudo knock intensity level is even greater than that seen at knock onset conditions. The larger amplitudes in these signals make the noise before the autoignition initiation point much less significant; however, the multiple frequencies are still easily seen for a short period of time, roughly 5-10 crank angle degrees, before they fade to only the 6.5 kHz signal. Again, because of the larger amplitude, this 6.5 kHz signal will actually appear to be smoother and contain less noise.

3.2.4 Further Exploration of Higher Frequency Bands in Cylinder Pressure

In combining the information from the three-tier plots regarding the multiple frequencies and the power spectra of the raw pressure traces, further bandpass filtering was completed. In addition to the original 6-7 kHz bandpass filter, a filter for the highest frequency band was used with a range of 15-20 kHz, as well as a filter that would encompass all of the frequencies with a range of 6-23 kHz.

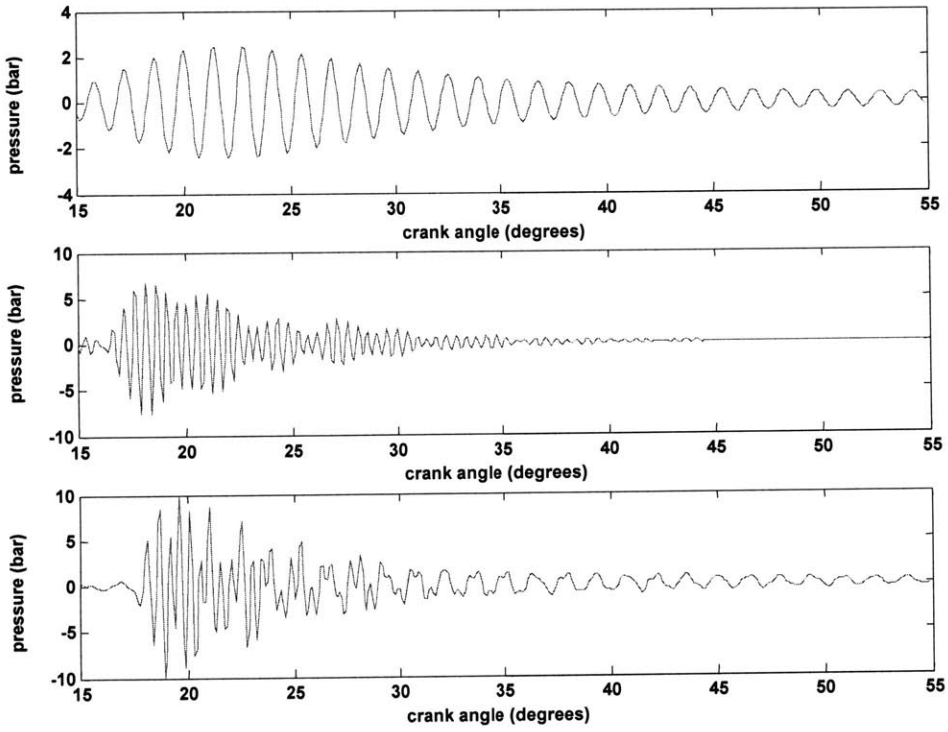

Figure 3. 16: Pressure Traces Bandpass Filtered with Multiple Frequency Bands including: 6-7 kHz (top), 15-20 kHz (middle), and 6-23 kHz (bottom) for a Heavily Knocking Spark Timing of 6° BTC

By looking at a combination of filtered pressure traces for the three different frequency bands as in Figure 3. 16, it can be seen that when the magnitude of knock intensity is large in one frequency band it is usually large in the other frequency bands as well. The magnitudes of the knock intensity levels vary greatly between the first and second frequency bands so knock intensity values across filters should not be compared. In general, cycles that meet the criteria for having autoignition events that lead to engine knock also have a very rapid build-up of oscillations that slowly diminish in the 15-20

kHz band as well. The most significant visual difference between the figures is that the traces filtered at the higher frequency band appear to have a smaller number of oscillations before reaching their maximum. This appears as a sharper, flatter front to the signal build-up. This sharper, flatter front also appears in the traces where both frequencies are included in the filter. Again, determining the difference between very heavy levels of knock and complete non-knock can be easily resolved visually with the use of any of these filters. The difficulty lies in determining the knock condition of those cycles that are near the knock onset point.

3.2.5 Microphone Signal Analysis

After a power spectrum analysis was completed on the microphone data, it was apparent that the same 6-7 kHz bandpass filter that was used for the raw cylinder pressure signal could be used to filter the microphone data as well. This power spectrum analysis result makes sense because of the filtering done by the equalizer prior to the signal being recorded. Figure 3. 17, Figure 3. 18, and Figure 3. 19 are plots of the filtered cylinder pressure signal superimposed over the filtered microphone signal. There is a strong correlation between these two sets even though there were differences in the amplitudes due to the level the microphone volume was set and due to a great deal more noise in the signal from other engine noises that occur at a 6-7 kHz frequency. There are more areas of high amplitude signal in the filtered microphone data, but usually the largest amplitude one correlates with the single high amplitude region in the filtered cylinder pressure trace.

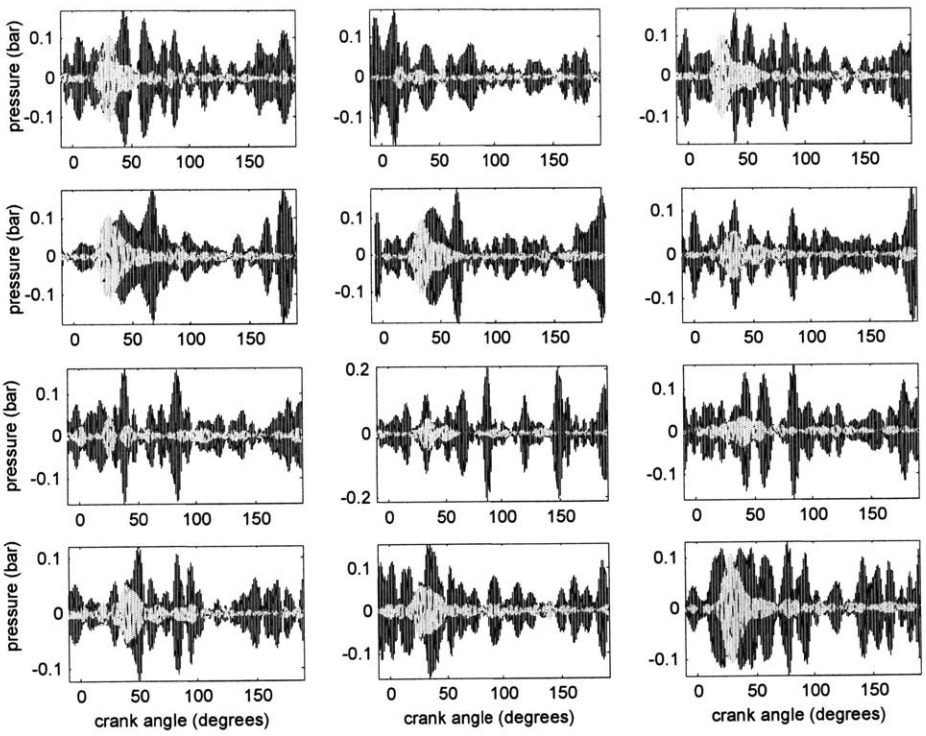

Figure 3. 17: Cylinder Pressure Trace Superimposed over Microphone Signal for a Non-Knocking Spark Timing of 0° BTC

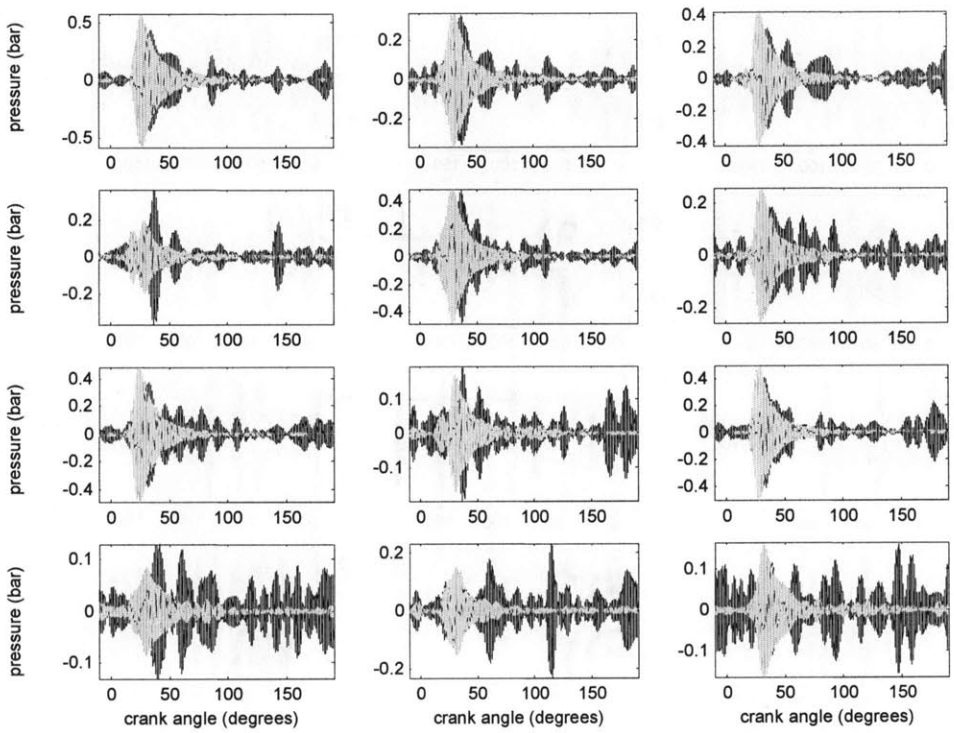

Figure 3. 18: Cylinder Pressure Trace Superimposed over Microphone Signal at the Knock Onset Spark Timing of 3° BTC

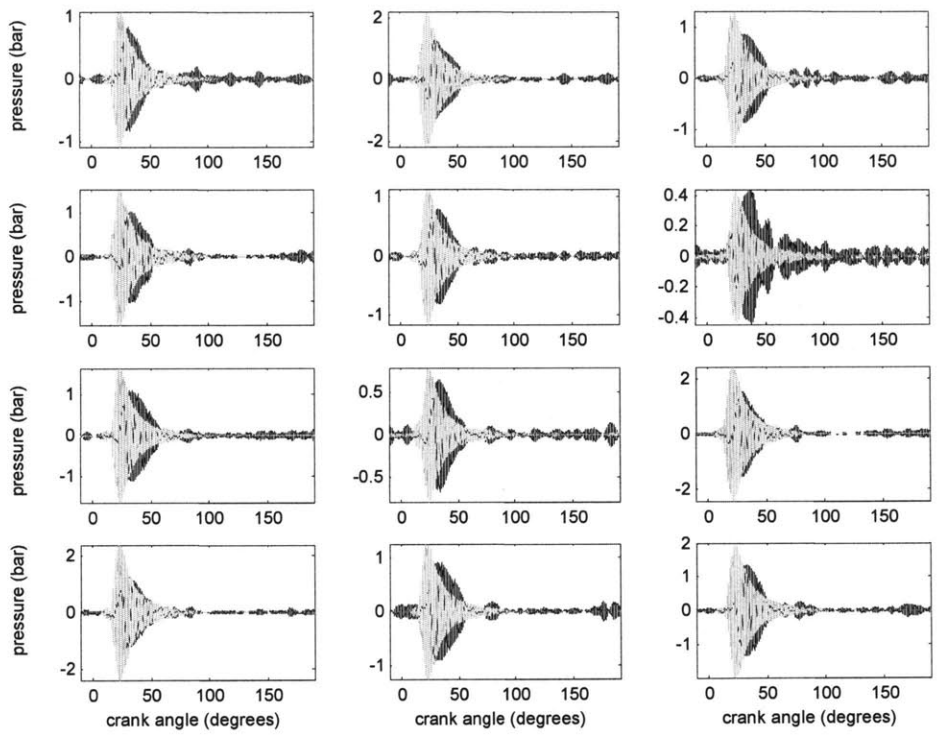

Figure 3. 19: Cylinder Pressure Trace Superimposed over Microphone Signal for a Heavily Knocking Spark Timing of 6° BTC

Additionally, the microphone data and cylinder pressure were compared by plotting cylinder pressure knock intensities versus microphone knock intensities. Microphone knock intensity was calculated using the same method as that for cylinder pressure knock intensity. An example of a partial set of these plots can be found in Figure 3. 20, Figure 3. 21, and Figure 3. 22 while those for all of the octane ratings can be found in the appendix. A linear trendline was then fit to each set of data as well as an R^2 value for each of the trendlines. Spark timings that are non-knocking have relatively low R^2 values for these trendline equations. When the spark timing of knock onset is reached, the R^2 value for the linear equation jumps to a higher value that is in the region or greater than 0.85. This shows a much more substantial linear relationship develops between the microphone knock intensity and the cylinder pressure knock intensity as knock onset is

reached. Figure 3. 23 shows the progression of the R^2 values across the spark timing ranges for the various octane ratings.

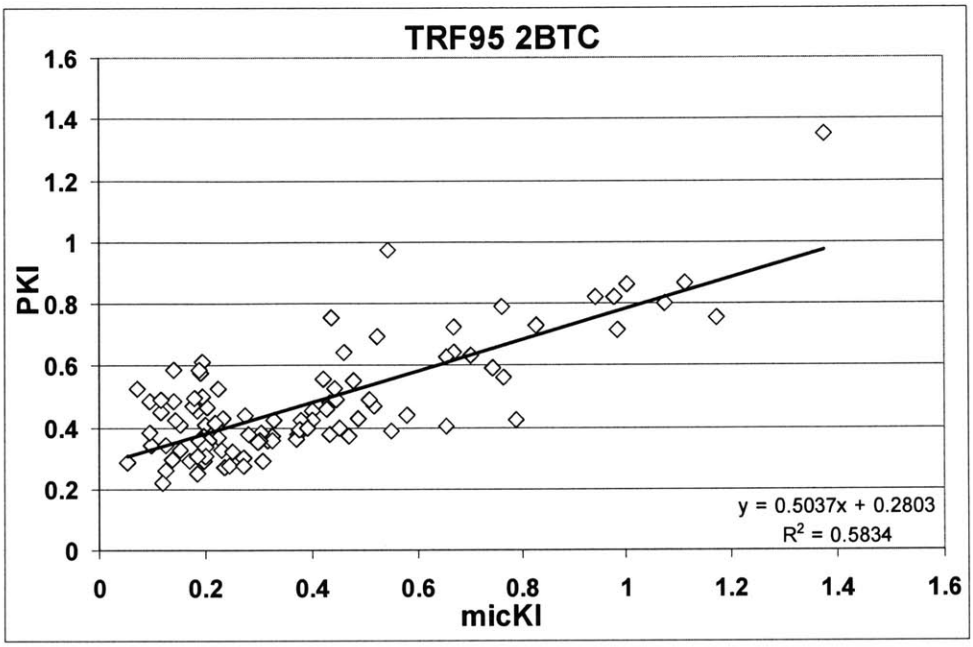

Figure 3. 20: Comparison of the Cylinder Pressure KI and Microphone KI for a Non-Knocking Spark Timing

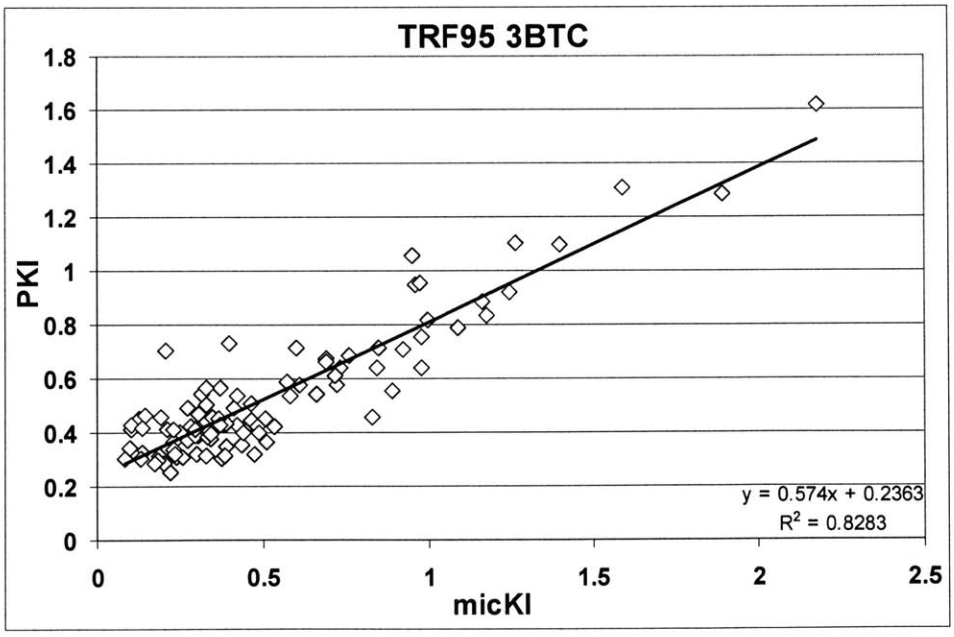

Figure 3. 21: Comparison of the Cylinder Pressure KI and Microphone KI at the Knock Onset Spark Timing

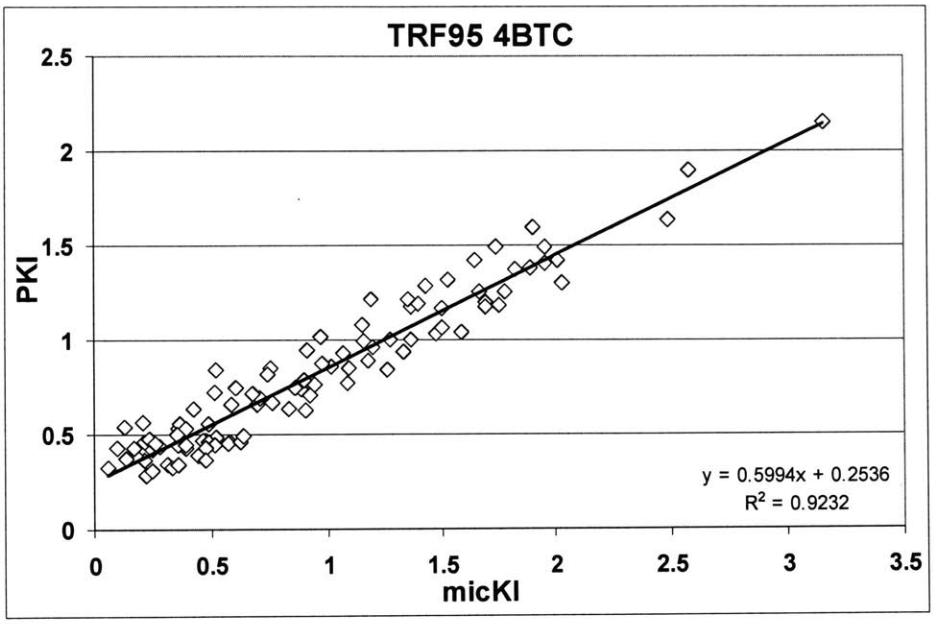

Figure 3. 22: Comparison of Cylinder Pressure KI and Microphone KI at a Heavier Knocking Spark Timing

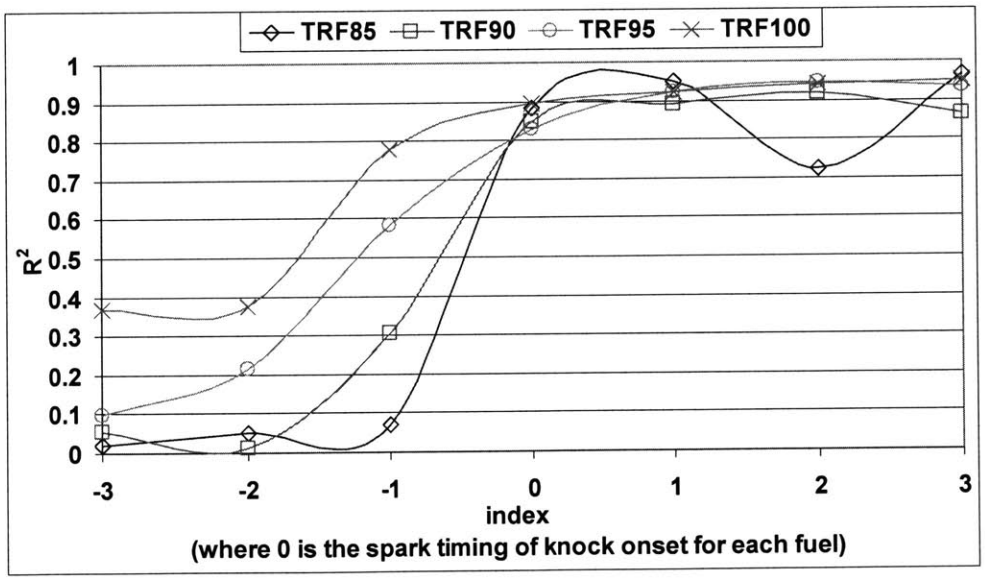

Figure 3. 23: Trends in R^2 Value for Each of the Four Tested Fuels

(page intentionally left blank)

CHAPTER 4: SUMMARY AND CONCLUSIONS

The data presented in this work confirms that the cylinder pressure signal contains multiple frequencies of interest. The first is near 6.5 kHz which is the resonant frequency of the cylinder. Another is near 17.5 kHz which is close to the third harmonic of the resonance frequency. While filtering is useful, using a smoothing technique to find a mean pressure trace and then subtracting it from the original pressure trace may be an adequate means of data processing for evaluation of the data.

Using either bandpass filtered data or mean removed pressure data, a knock intensity can be determined that gives significant insight into the type of autoignition event that may have occurred during a cycle and whether or not that autoignition event will lead to engine knock. Microphone signal data can also be bandpass filtered and knock intensities can be calculated from this data also providing information on the type of autoignition during a cycle. This bandpass filtered microphone data has similar bursts of oscillations to those found in the bandpass filtered pressure traces.

The figures regarding the number of oscillations before peak in a bandpass filtered pressure trace support the ideas from previous work that the end gas contains one or more hot spots that autoignite causing pressure gradients that can trigger rapid pressure oscillations. These pressure oscillations can cause block and head vibrations that lead to audible noise outside the engine. The number of oscillations before peak amplitude is related to how rapidly the pressure oscillations are able to build up, while the knock intensity is related to the amount of energy available for release as noise for that particular cycle.

The mean removed pressure traces show that there is a gradual build-up to more intense autoigniting cycles as conditions transition from non-knocking to knock onset and on to heavier knock. This transition includes a period of higher frequency pressure waves that set up the autoignition process, presumably in a similar manner to those seen in the video frames from Pan and Sheppard [7]. These higher frequency pressure waves then decay to a single base frequency of 6.5 kHz for the tests completed in this work.

There are three promising methods that could potentially be used in for determining knock onset without the need to have an operator constantly sitting at the engine and listening. The first uses plots of the knock intensity versus the number of oscillations before the peak of a lowest frequency (in this instance a 6-7 kHz) bandpass filtered pressure trace. On these plots, cycles begin to appear in the region of KI greater than 1 bar and a short 5-10 oscillation build-up to peak. The second method looks at the average KI over all the cycles and the average $(dP/d\theta)_{max}$ over all cycles. Using the data taken thus far, trends have shown that knock onset correlates with an average KI of ~0.4 bar and an average $(dP/d\theta)_{max}$ of ~10 bar/ °CA. The third possible method uses the R^2 values from linear trendlines on plots of cylinder pressure knock intensity versus microphone signal knock intensity. As the R^2 value takes a jump from distinctively lower values into a region of values greater than 0.85, knock onset occurs.

Future work should consist of more extensive microphone signal testing and analysis as well as an expansion of test fuels. Additional microphone data is needed to confirm the relationship between the various knock intensities. Moving the microphone to various locations around the outside of the engine including different heights could possibly give insight into where the end gas or hot spots might be more prevalent and may lead to a better description of what is physically taking place in the cylinder. Further processing of the microphone data in various manners could also be done in order to look for any further in-cylinder details. As for fuels, in addition to the TRFs tested, PRFs should also be investigated in order to determine if the same trends are seen for a different type of fuel. Once trends have been confirmed with PRFs, unleaded test gasolines of various octane ratings should be used in order to confirm that fuels more like those used in the real world also behave as predicted.

REFERENCES

[1] Heywood, J.B., *Internal Combustion Engine Fundamentals,* McGraw Hill Inc., New York, 1988.

[2] Lee, J., Hwang, S., Lim, J., et al., "A New Knock-Detection Method using Cylinder Pressure, Block Vibration and Sound Pressure Signals from a SI Engine," SAE 981436.

[3] Kaneyasu, M., et al., "Engine Knock Detection Using Multi-Spectrum Method," SAE 920702.

[4] Chiriac, R., Radu, B., and Apostolescu, N., "Defining Knock Characteristics and Autoignition Conditions of LPG with a Possible Correlation for the Control Strategy in a SI Engine," SAE 2006-01-0227.

[5] Grandin, B., Denbratt, I., et al., "Heat Release in the End-Gas Prior to Knock in Lean, Rich and Stoichiometric Mixtures With and Without EGR," SAE 2002-01-0239.

[6] Bradley, D., Morley, C., et al., "Amplified Pressure Waves During Autoignition: Relevance to CAI Engines," SAE 2002-01-2868.

[7] Konig, G. and Sheppard, C.G.W., "End Gas Autoignition and Knock in a Spark Ignition Engine," SAE 902135.

[8] Pan, J. and Sheppard, C.G.W., "A Theoretical and Experimental Study of the Modes of End Gas Autoignition Leading to Knock in S.I.Engines," SAE 942060.

[9] Topinka, J., *Knock Behavior of a Lean-Burn, H_2 and CO Enhanced, SI Gasoline Engine Concept*, M.S. Thesis, MIT, May 2002.

[10] Gerty, M.D., *Effects of Operating Conditions, Compression Ratio, and Gasoline, Reformate on SI Engine Knock Limits*, M.S. Thesis, MIT, May 2005.

(page intentionally left blank)

APPENDIX: ADDITIONAL FIGURES

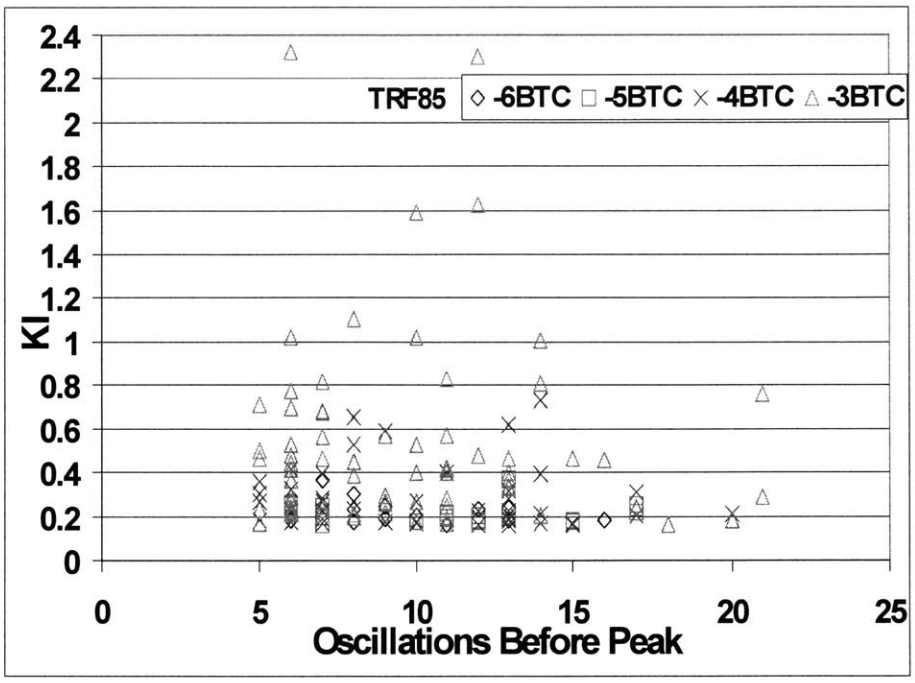
TRF85
-6BTC
-5BTC
-4BTC
-3BTC
KI
Oscillations Before Peak
0
0.2
0.4
0.6
0.8
1
1.2
1.4
1.6
1.8
2
2.2
2.4
0
5
10
15
20
25

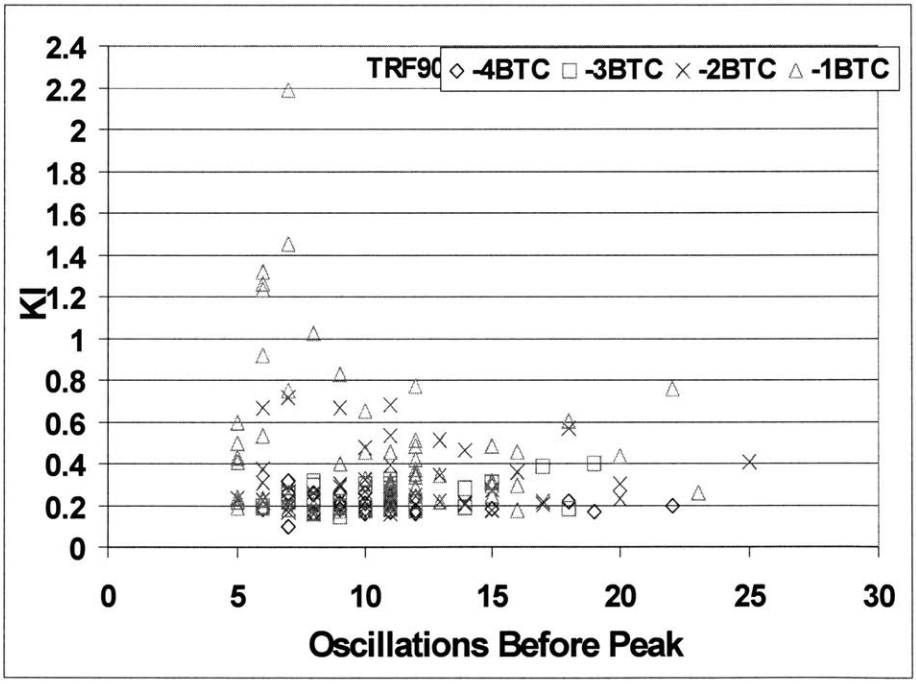
TRF90
-4BTC
-3BTC
-2BTC
-1BTC
KI
Oscillations Before Peak
0
0.2
0.4
0.6
0.8
1
1.2
1.4
1.6
1.8
2
2.2
2.4
0
5
10
15
20
25
30

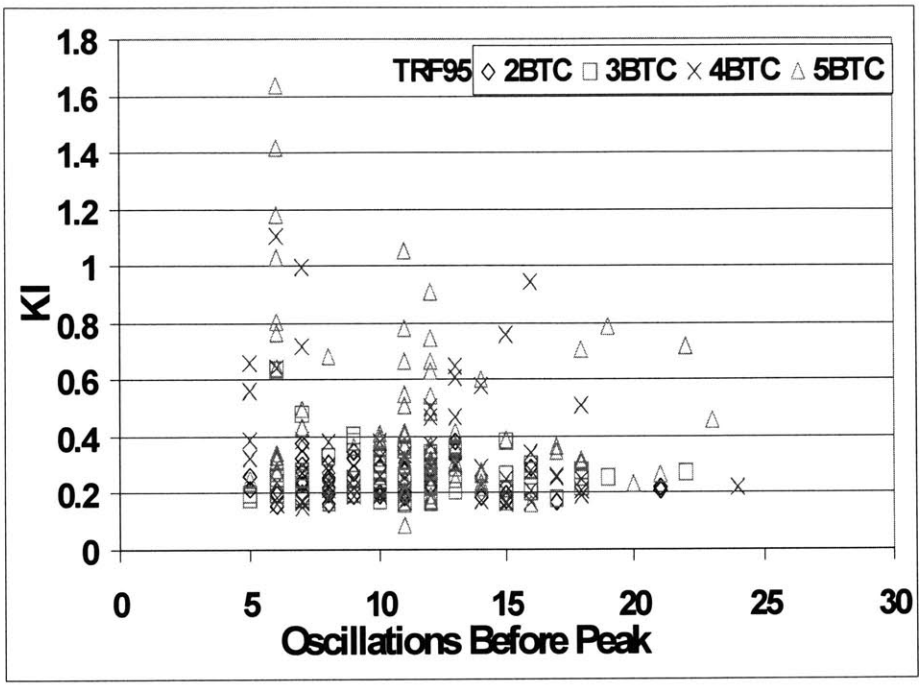
TRF95
2BTC
3BTC
4BTC
5BTC
KI
Oscillations Before Peak
0
0.2
0.4
0.6
0.8
1
1.2
1.4
1.6
1.8
0
5
10
15
20
25
30

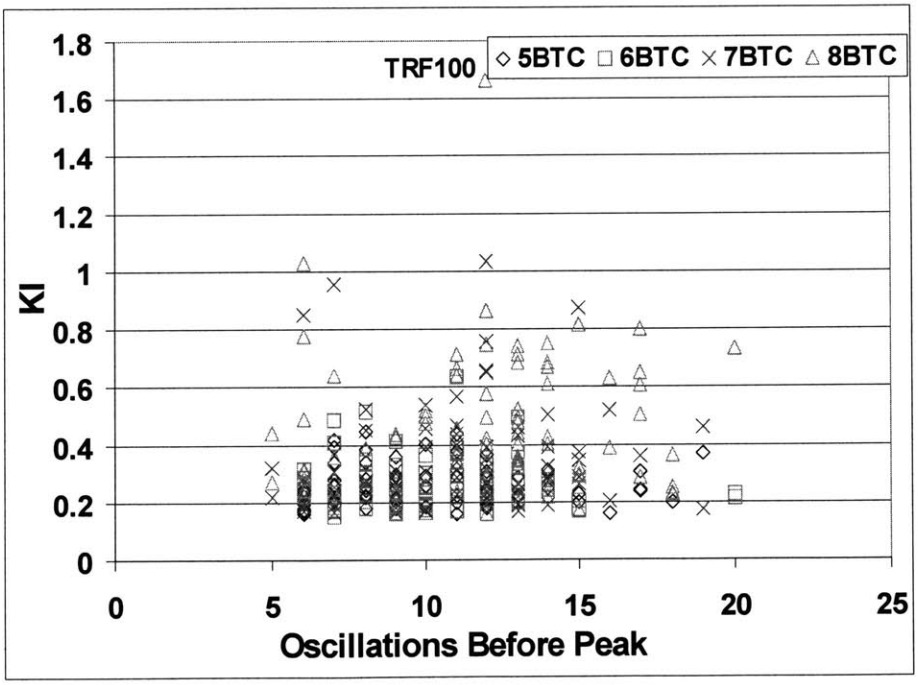
TRF100
5BTC
6BTC
7BTC
8BTC
KI
Oscillations Before Peak
0
0.2
0.4
0.6
0.8
1
1.2
1.4
1.6
1.8
0
5
10
15
20
25

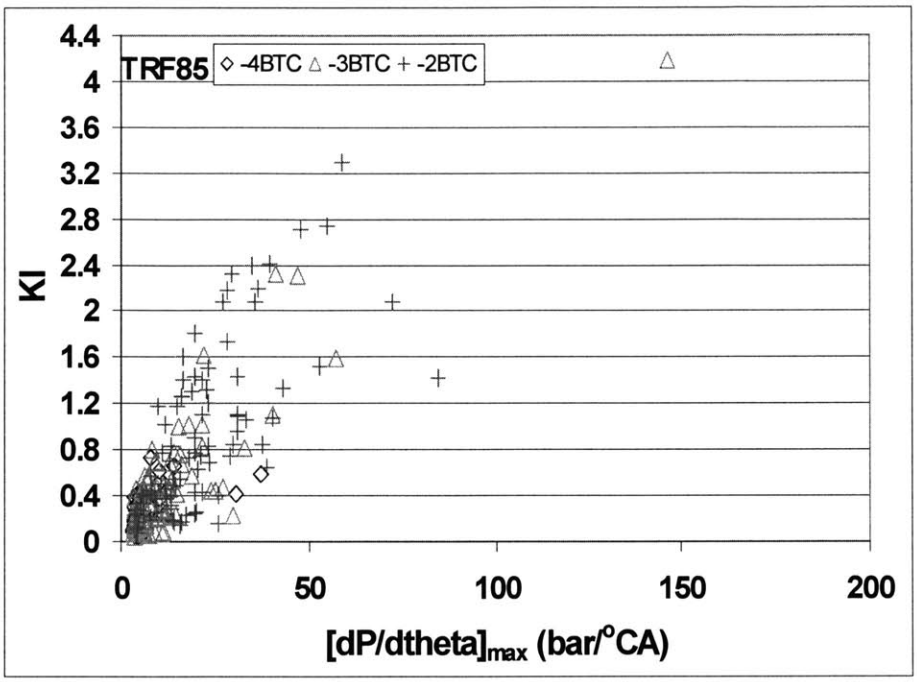
TRF85
◇ -4BTC △ -3BTC + -2BTC
KI
4.4
4
3.6
3.2
2.8
2.4
2
1.6
1.2
0.8
0.4
0
0
50
100
150
200
[dP/dtheta]max (bar/°CA)

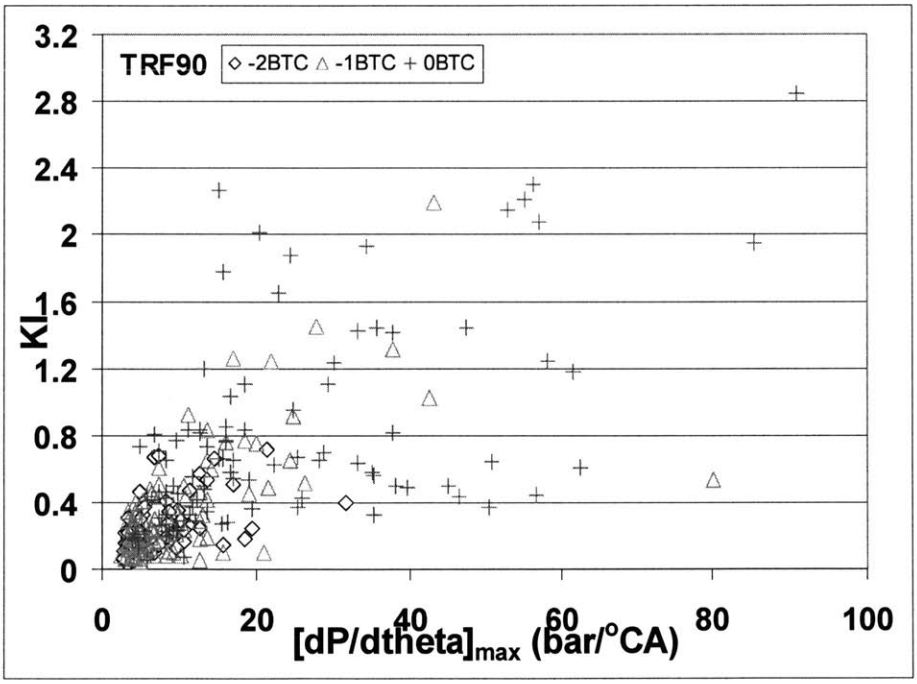
TRF90
◇ -2BTC △ -1BTC + 0BTC
KI
3.2
2.8
2.4
2
1.6
1.2
0.8
0.4
0
0
20
40
60
80
100
[dP/dtheta]max (bar/°CA)

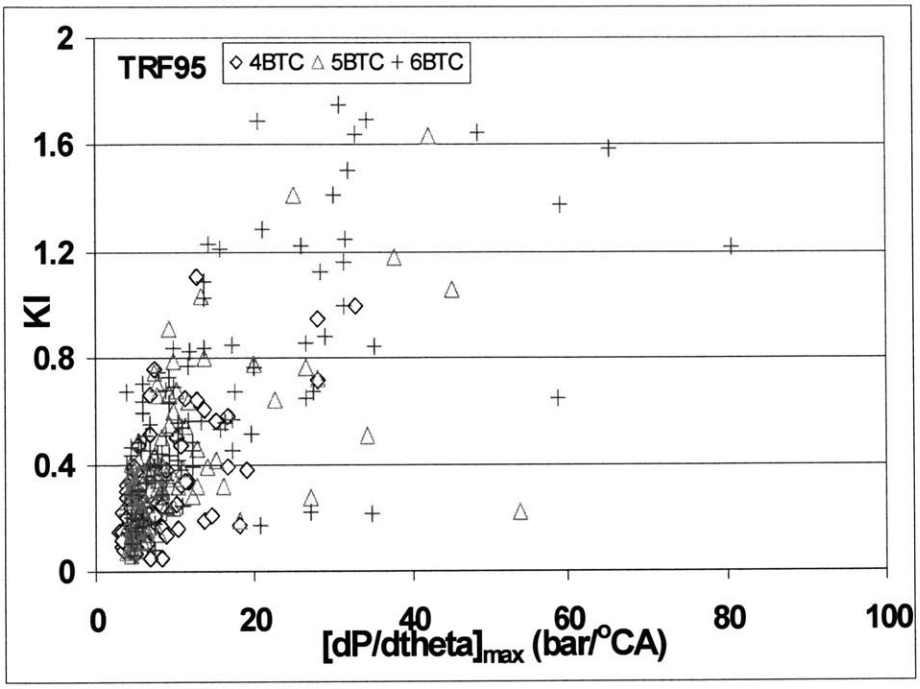
TRF95
◇ 4BTC △ 5BTC + 6BTC
KI
2
1.6
1.2
0.8
0.4
0
0
20
40
60
80
100
[dP/dtheta]max (bar/°CA)

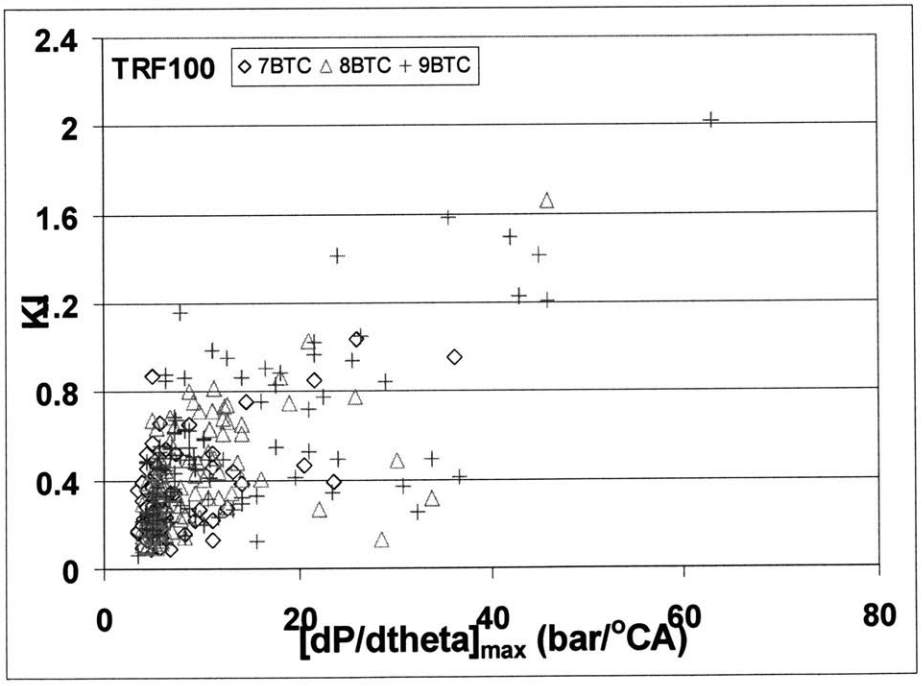
TRF100
◇ 7BTC △ 8BTC + 9BTC
KI
2.4
2
1.6
1.2
0.8
0.4
0
0
20
40
60
80
[dP/dtheta]max (bar/°CA)

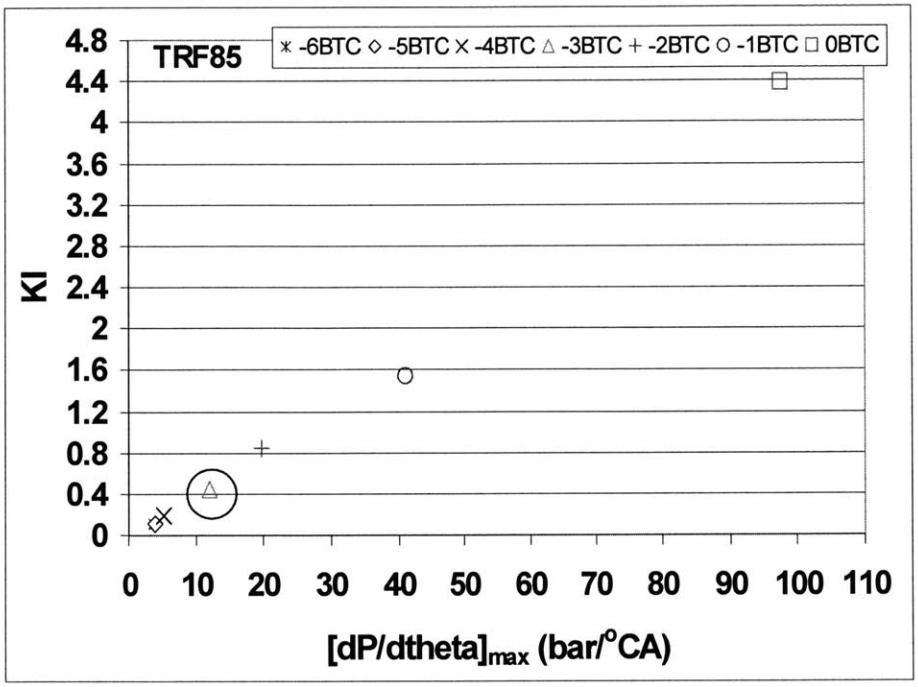
TRF85
-6BTC -5BTC -4BTC -3BTC -2BTC -1BTC 0BTC
KI
4.8
4.4
4
3.6
3.2
2.8
2.4
2
1.6
1.2
0.8
0.4
0
0 10 20 30 40 50 60 70 80 90 100 110
[dP/dtheta]max (bar/°CA)

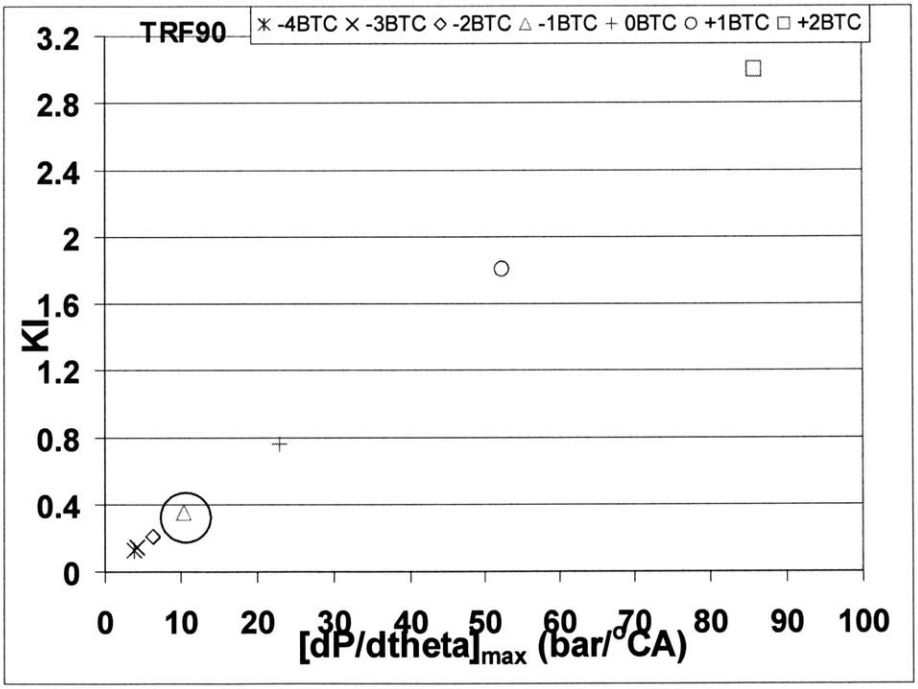
TRF90
-4BTC -3BTC -2BTC -1BTC 0BTC +1BTC +2BTC
KI
3.2
2.8
2.4
2
1.6
1.2
0.8
0.4
0
0 10 20 30 40 50 60 70 80 90 100
[dP/dtheta]max (bar/°CA)

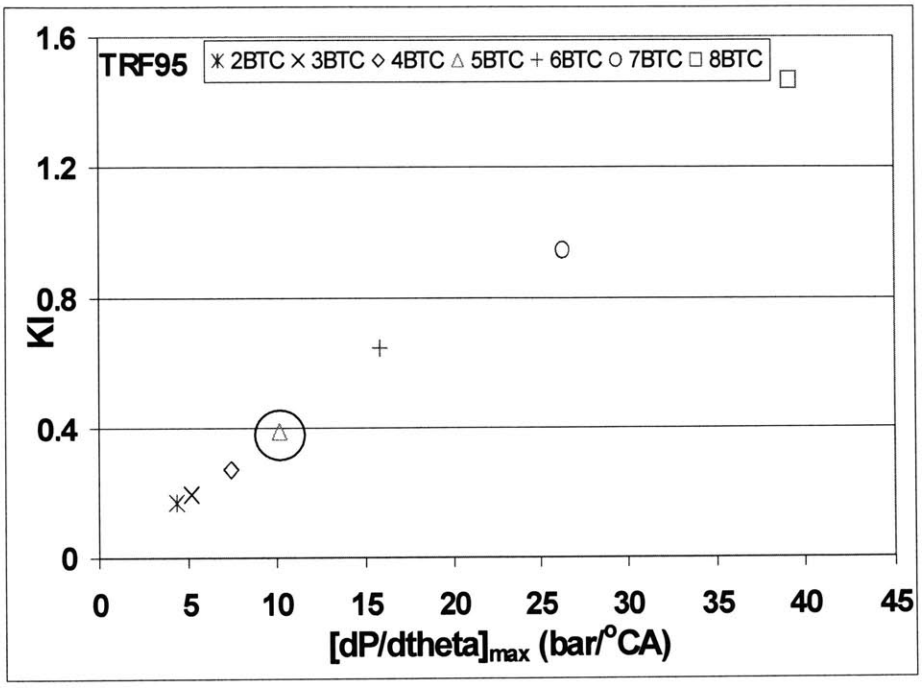
TRF95
✳ 2BTC × 3BTC ◇ 4BTC △ 5BTC + 6BTC ○ 7BTC □ 8BTC
1.6
1.2
0.8
0.4
0
KI
0
5
10
15
20
25
30
35
40
45
[dP/dtheta]max (bar/°CA)

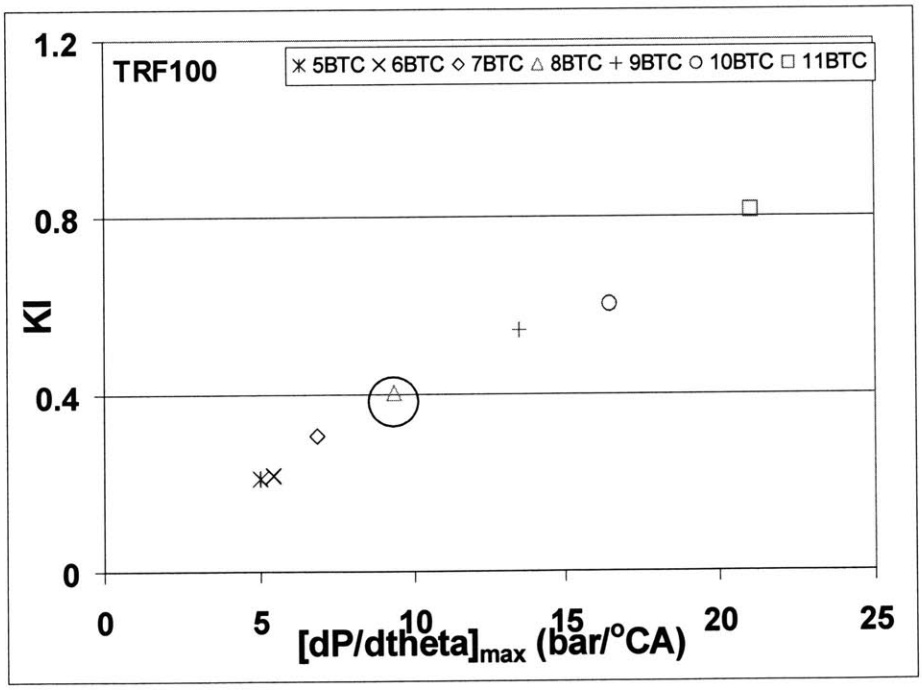
TRF100
✳ 5BTC × 6BTC ◇ 7BTC △ 8BTC + 9BTC ○ 10BTC □ 11BTC
1.2
0.8
0.4
0
KI
0
5
10
15
20
25
[dP/dtheta]max (bar/°CA)

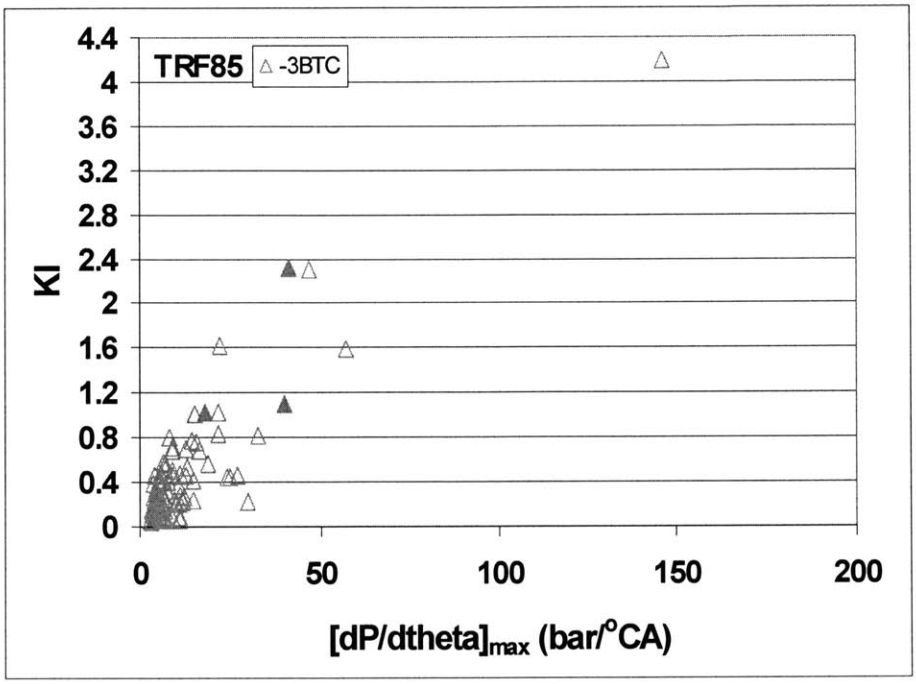
TRF85
-3BTC
KI
4.4
4
3.6
3.2
2.8
2.4
2
1.6
1.2
0.8
0.4
0
0
50
100
150
200
[dP/dtheta]max (bar/°CA)

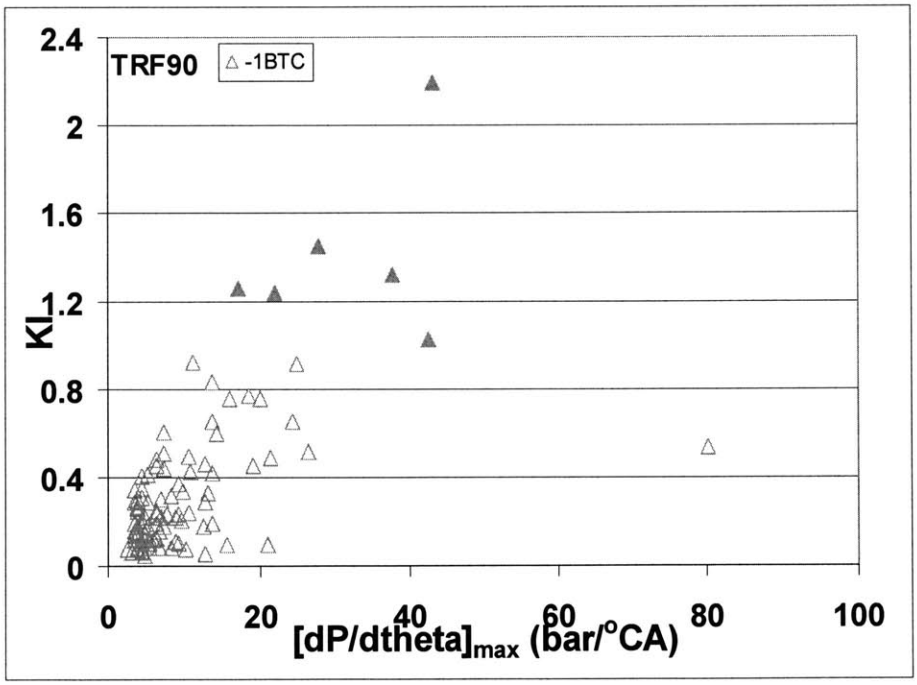
TRF90
-1BTC
KI
2.4
2
1.6
1.2
0.8
0.4
0
0
20
40
60
80
100
[dP/dtheta]max (bar/°CA)

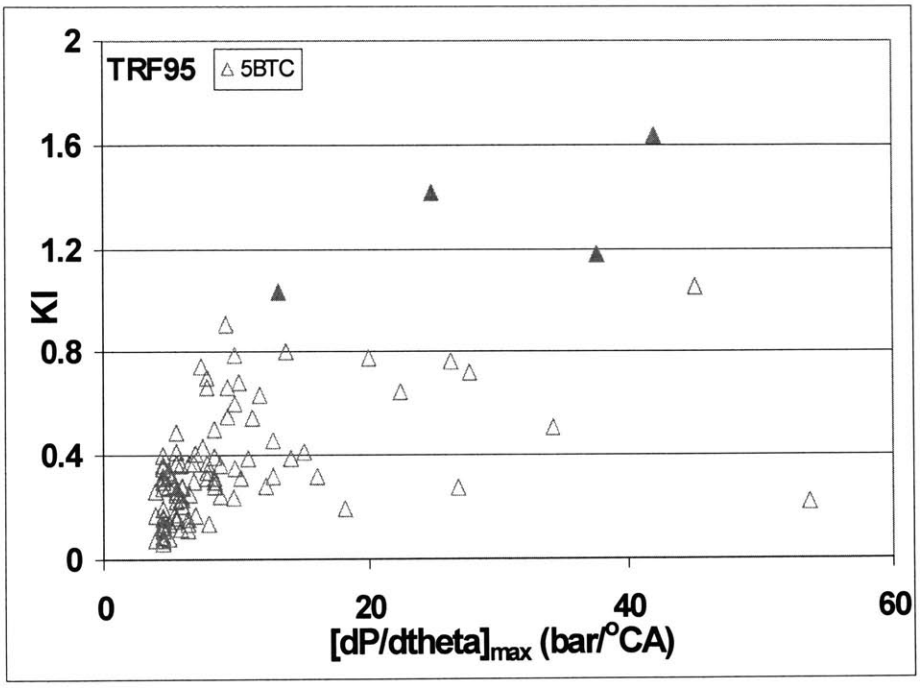
TRF95
5BTC
KI
2
1.6
1.2
0.8
0.4
0
0
20
40
60
[dP/dtheta]max (bar/°CA)

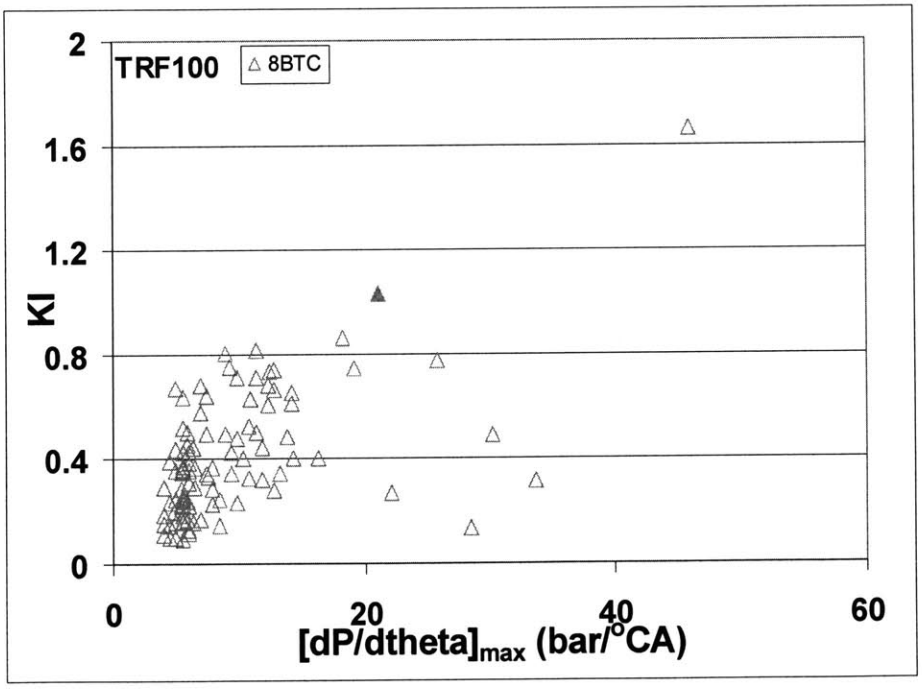
TRF100
8BTC
KI
2
1.6
1.2
0.8
0.4
0
0
20
40
60
[dP/dtheta]max (bar/°CA)

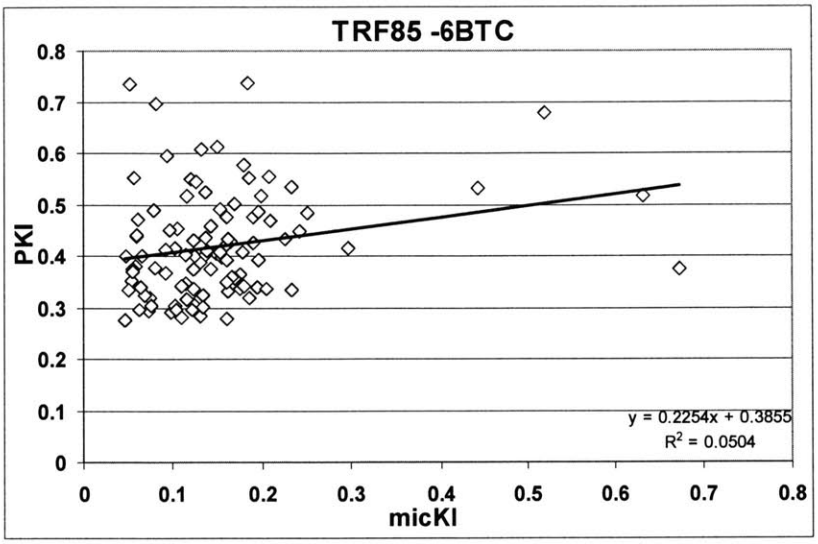
TRF85 -6BTC
PKI
micKI
y = 0.2254x + 0.3855
R2 = 0.0504
0
0.1
0.2
0.3
0.4
0.5
0.6
0.7
0.8

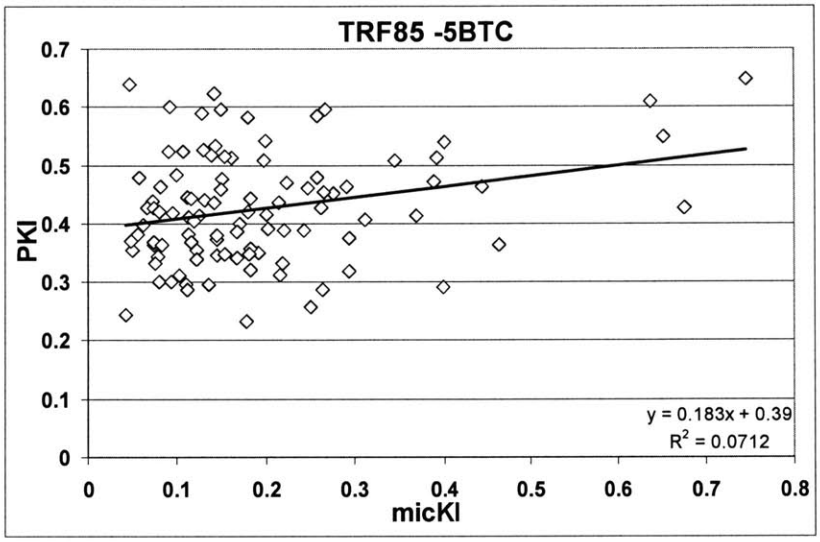
TRF85 -5BTC
PKI
micKI
y = 0.183x + 0.39
R2 = 0.0712
0
0.1
0.2
0.3
0.4
0.5
0.6
0.7
0.8

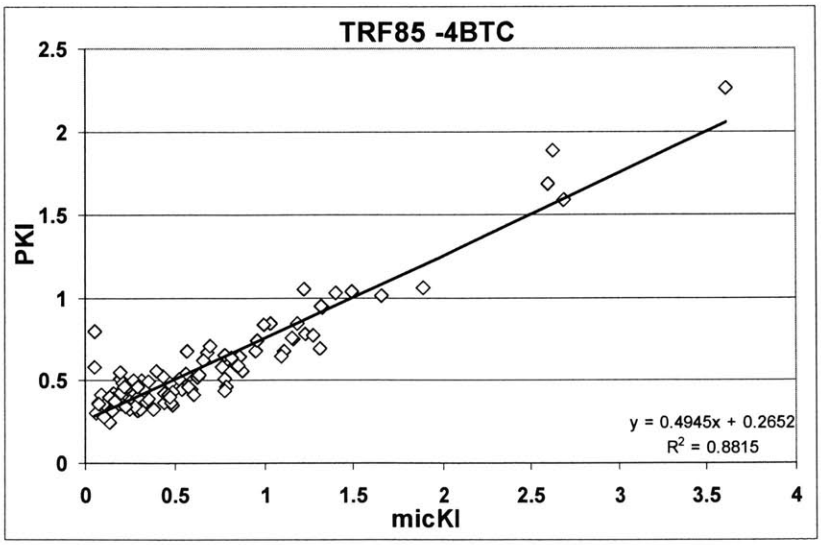
TRF85 -4BTC
PKI
micKI
y = 0.4945x + 0.2652
R2 = 0.8815
0
0.5
1
1.5
2
2.5
3
3.5
4

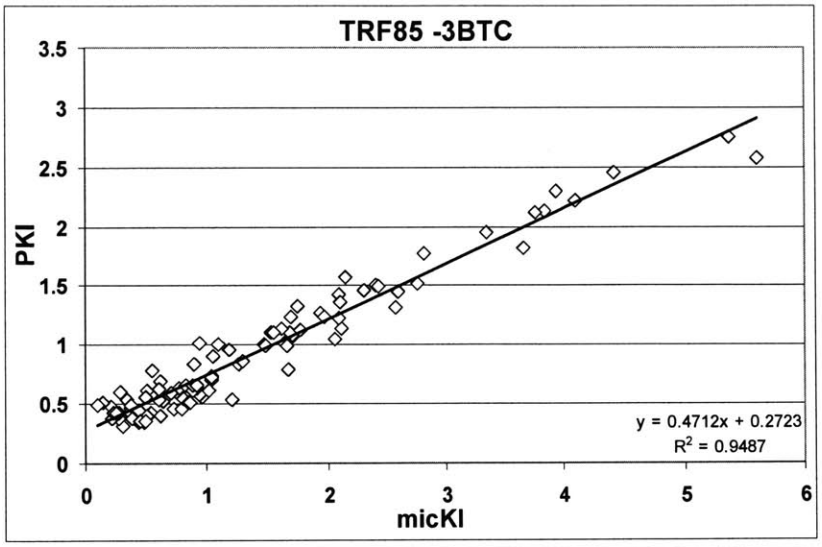
TRF85 -3BTC
PKI
micKI
y = 0.4712x + 0.2723
R2 = 0.9487

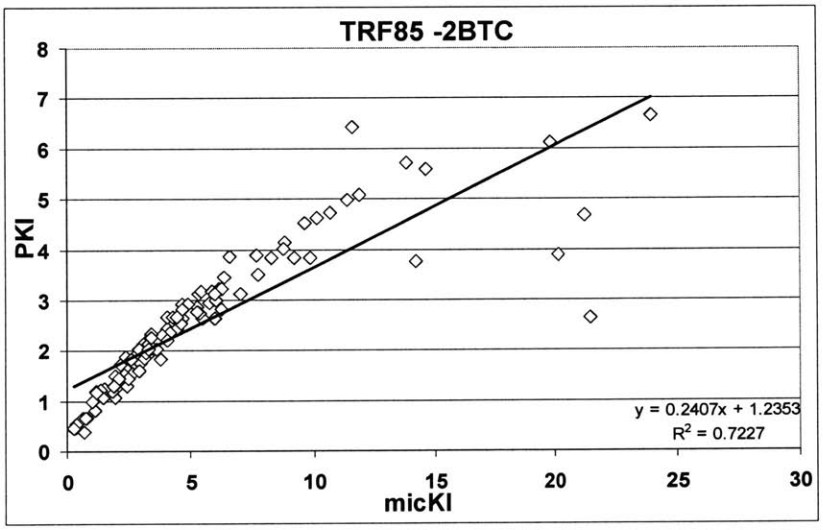
TRF85 -2BTC
PKI
micKI
y = 0.2407x + 1.2353
R2 = 0.7227

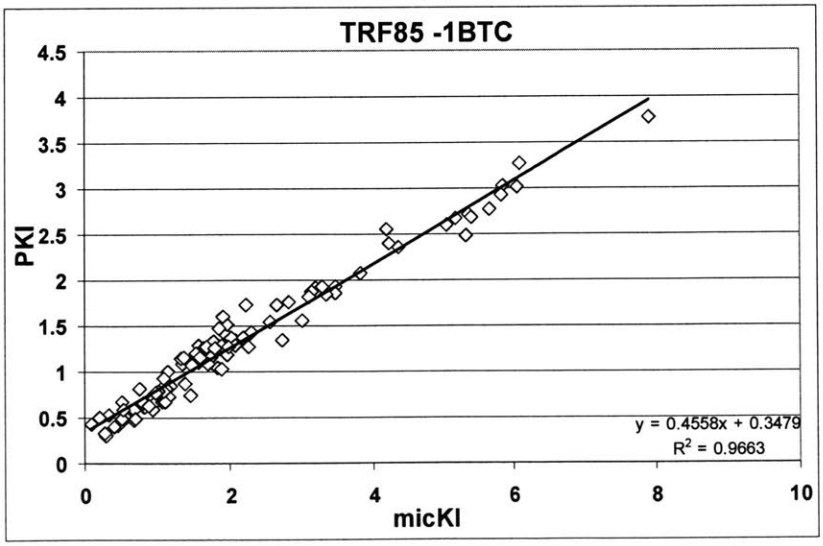
TRF85 -1BTC
PKI
micKI
y = 0.4558x + 0.3479
R2 = 0.9663

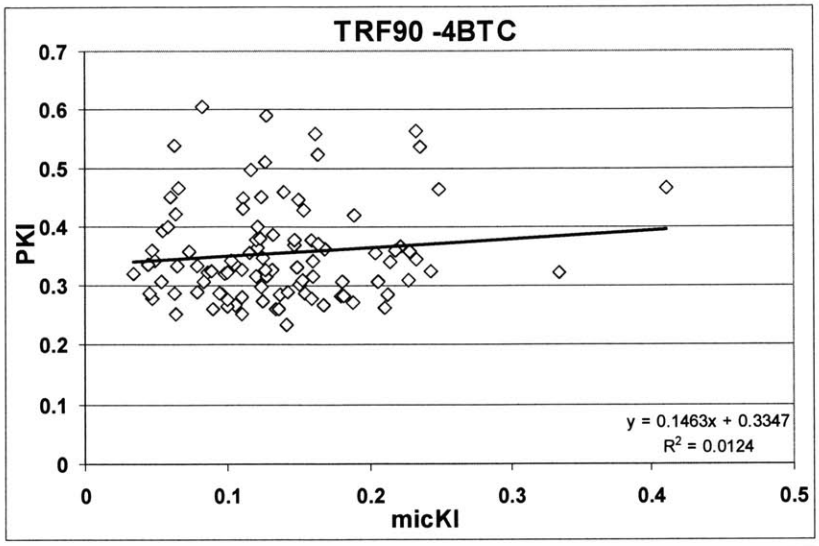
TRF90 -4BTC
PKI
micKI
y = 0.1463x + 0.3347
R2 = 0.0124
0
0.1
0.2
0.3
0.4
0.5
0.6
0.7

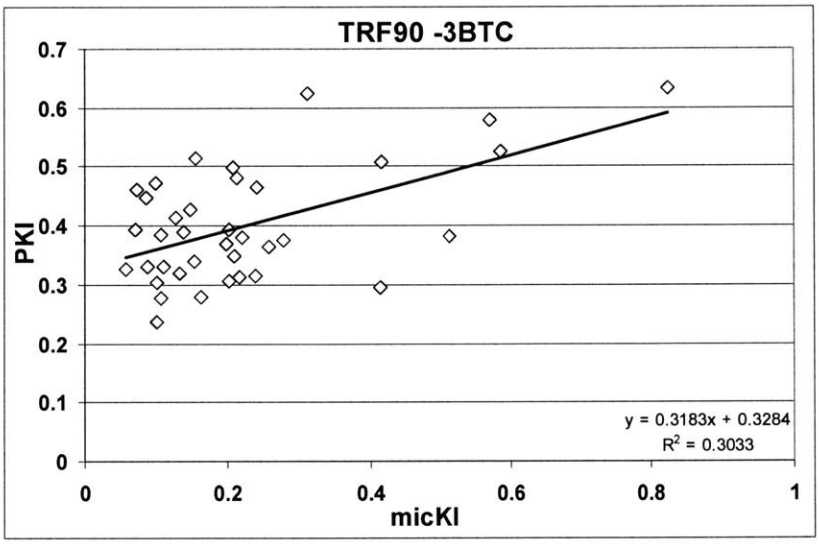
TRF90 -3BTC
PKI
micKI
y = 0.3183x + 0.3284
R2 = 0.3033
0
0.2
0.4
0.6
0.8
1

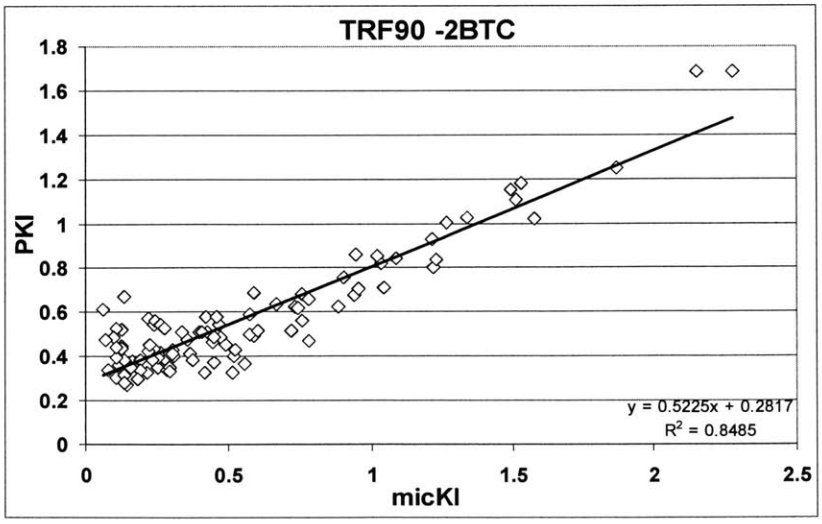
TRF90 -2BTC
PKI
micKI
y = 0.5225x + 0.2817
R2 = 0.8485
0
0.5
1
1.5
2
2.5

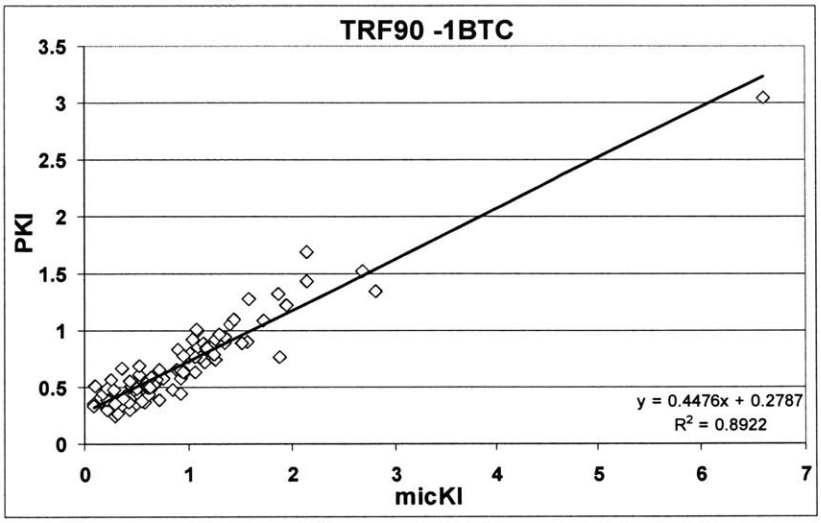
TRF90 -1BTC
PKI
micKI
y = 0.4476x + 0.2787
R² = 0.8922

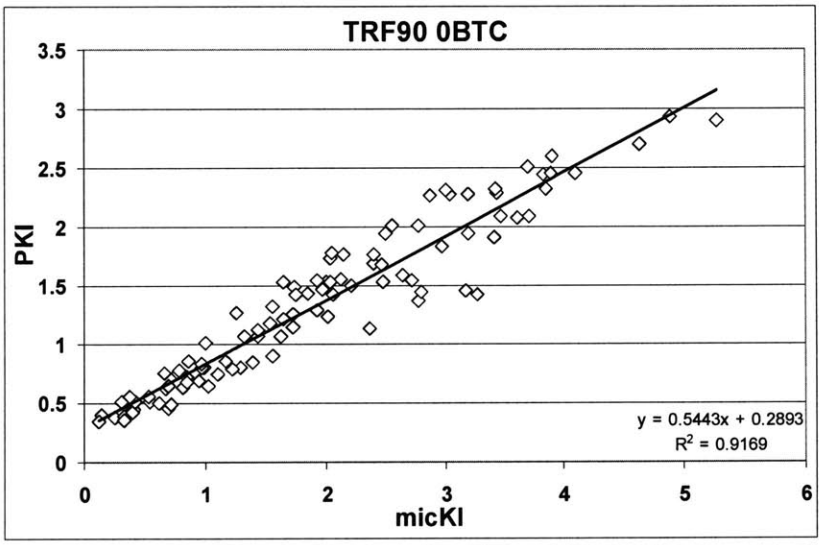
TRF90 0BTC
PKI
micKI
y = 0.5443x + 0.2893
R² = 0.9169

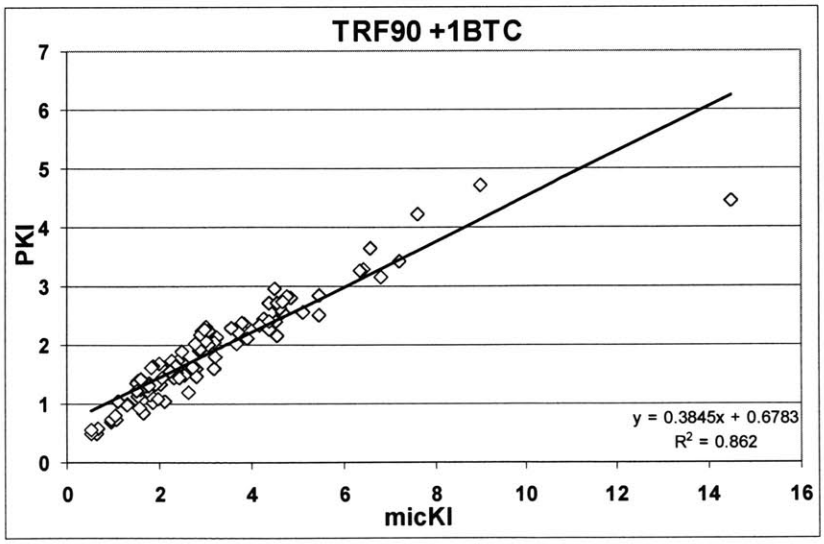
TRF90 +1BTC
PKI
micKI
y = 0.3845x + 0.6783
R² = 0.862

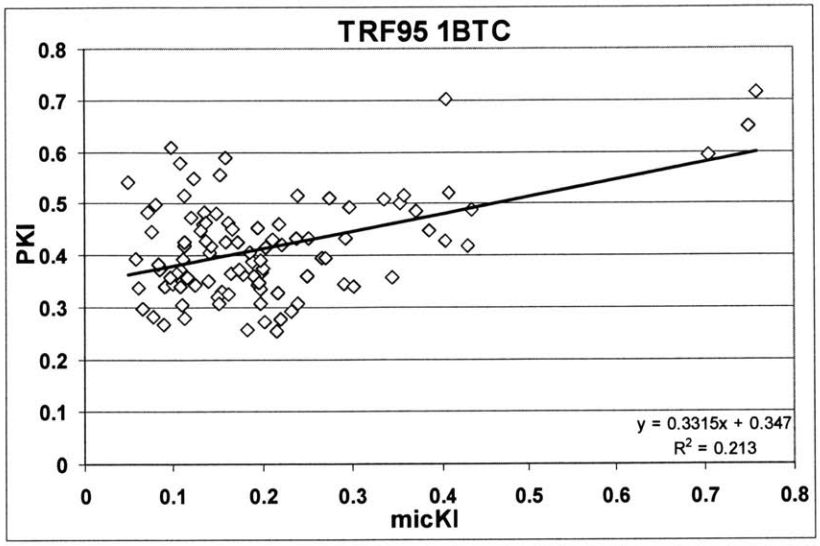
TRF95 1BTC
PKI
micKI
y = 0.3315x + 0.347
R2 = 0.213
0
0.1
0.2
0.3
0.4
0.5
0.6
0.7
0.8

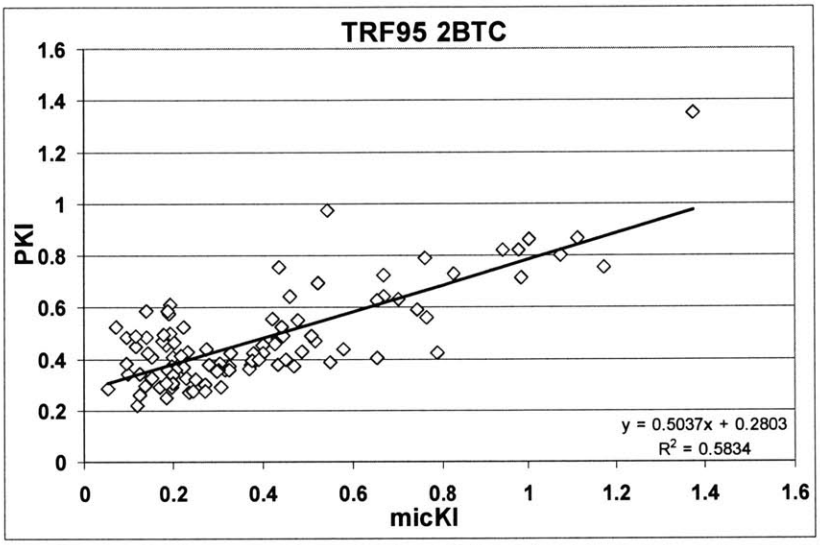
TRF95 2BTC
PKI
micKI
y = 0.5037x + 0.2803
R2 = 0.5834
0
0.2
0.4
0.6
0.8
1
1.2
1.4
1.6

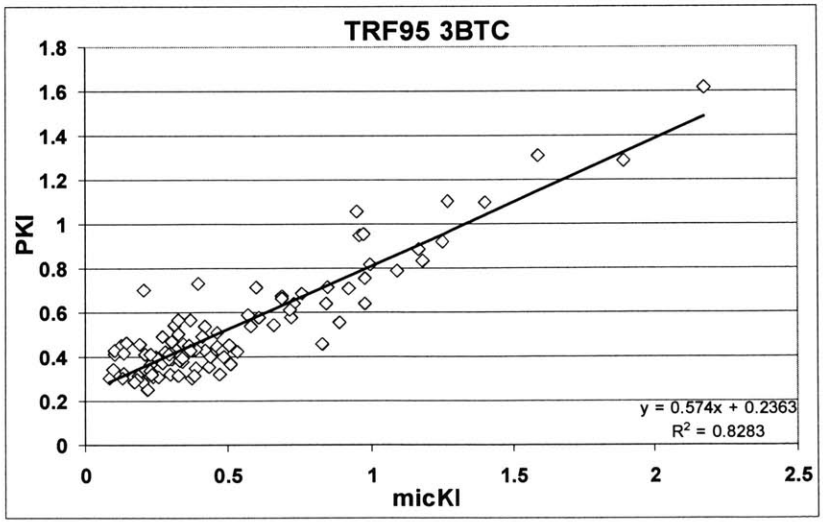
TRF95 3BTC
PKI
micKI
y = 0.574x + 0.2363
R2 = 0.8283
0
0.5
1
1.5
2
2.5

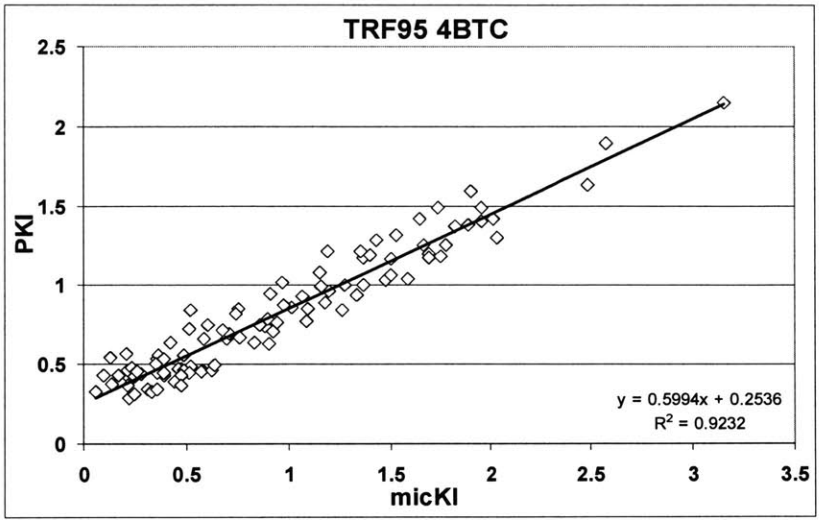
TRF95 4BTC
PKI
micKI
y = 0.5994x + 0.2536
R2 = 0.9232
0
0.5
1
1.5
2
2.5
3
3.5

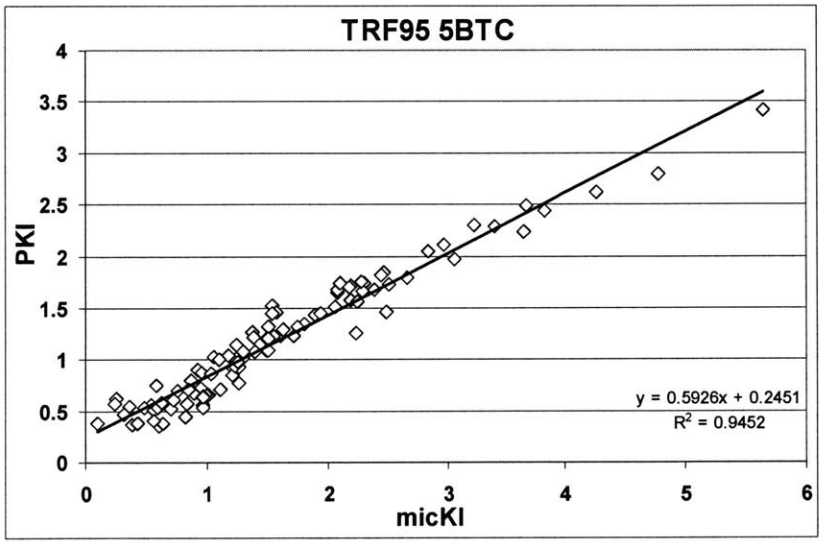
TRF95 5BTC
PKI
micKI
y = 0.5926x + 0.2451
R2 = 0.9452
0
1
2
3
4
5
6

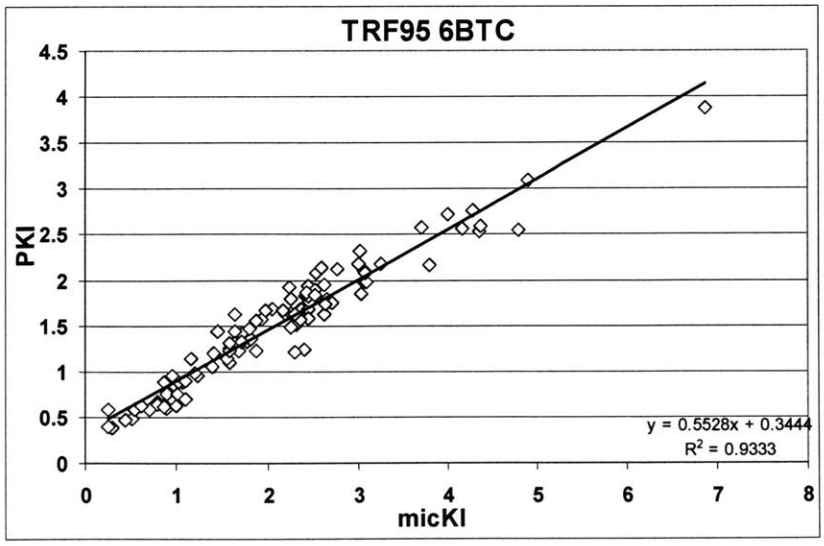
TRF95 6BTC
PKI
micKI
y = 0.5528x + 0.3444
R2 = 0.9333
0
1
2
3
4
5
6
7
8

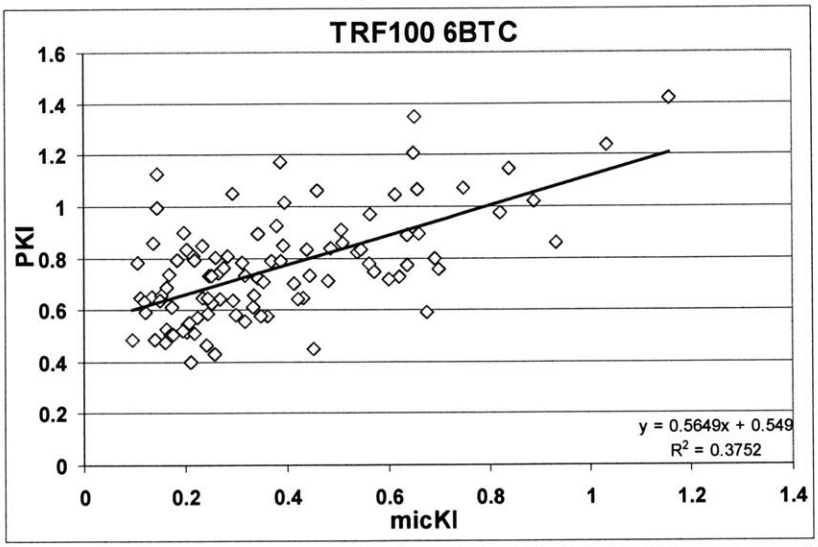
TRF100 6BTC
PKI
micKI
y = 0.5649x + 0.549
R2 = 0.3752
0
0.2
0.4
0.6
0.8
1
1.2
1.4
1.6

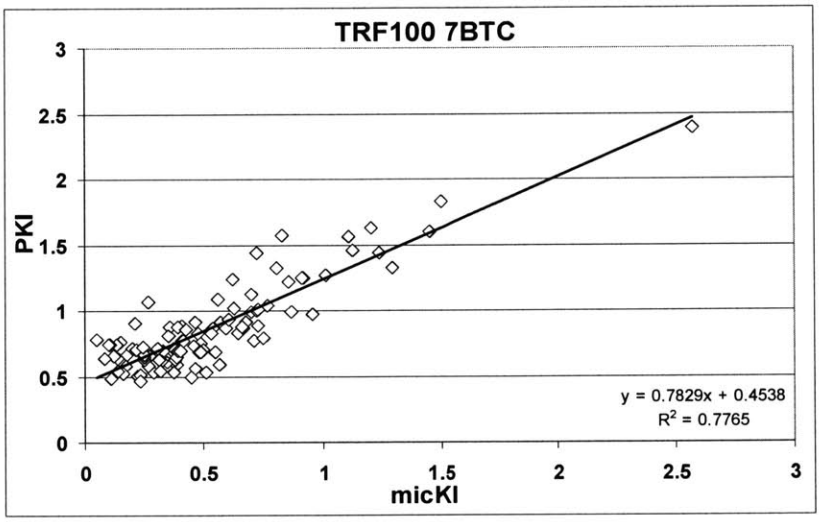
TRF100 7BTC
PKI
micKI
y = 0.7829x + 0.4538
R2 = 0.7765
0
0.5
1
1.5
2
2.5
3

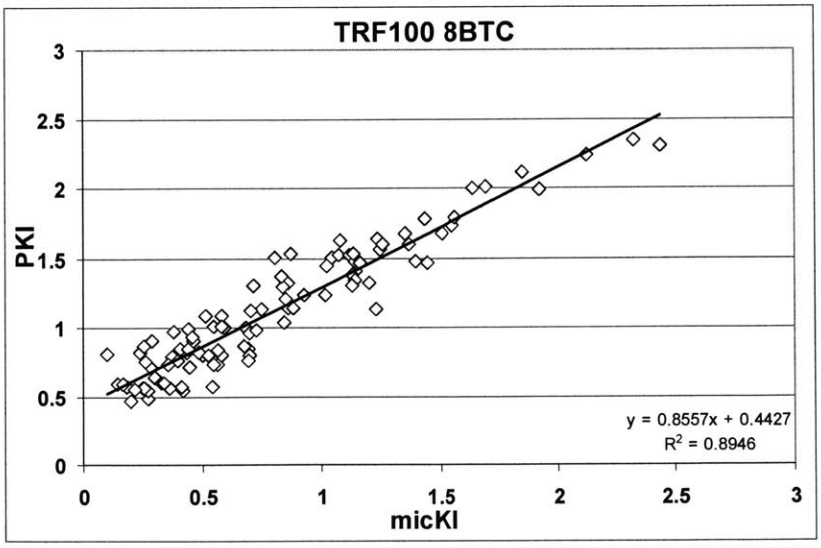
TRF100 8BTC
PKI
micKI
y = 0.8557x + 0.4427
R2 = 0.8946
0
0.5
1
1.5
2
2.5
3

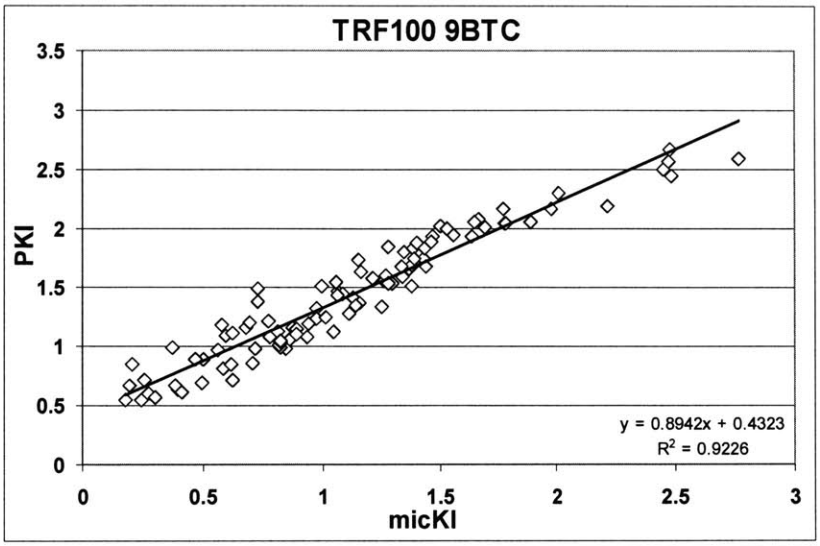
TRF100 9BTC
PKI
micKI
y = 0.8942x + 0.4323
R2 = 0.9226
0
0.5
1
1.5
2
2.5
3
3.5

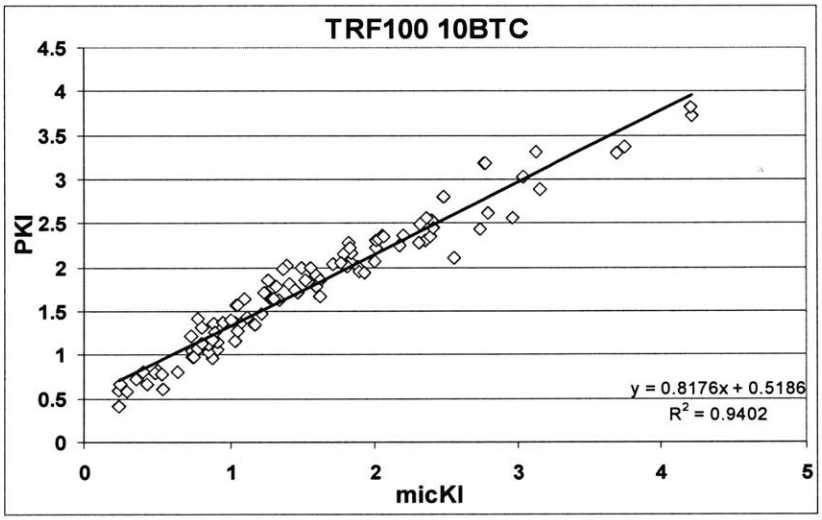
TRF100 10BTC
PKI
micKI
y = 0.8176x + 0.5186
R2 = 0.9402
0
0.5
1
1.5
2
2.5
3
3.5
4
4.5
5

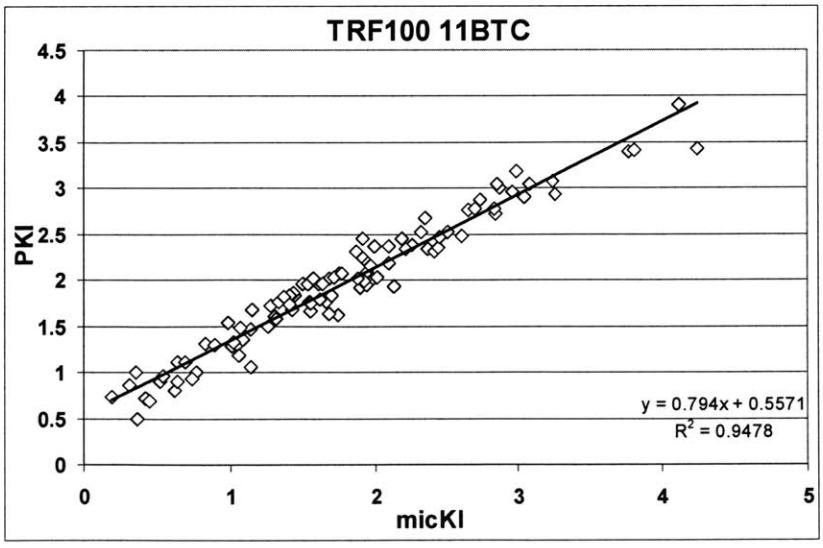
TRF100 11BTC
PKI
micKI
y = 0.794x + 0.5571
R2 = 0.9478
0
0.5
1
1.5
2
2.5
3
3.5
4
4.5
5

(page intentionally left blank)